Spring 5-2019

Development of a One-Equation Turbulence Model Based on k-ϵ Closure and its Extension for Computing Transitional Flows by Including an Intermittency Transport Equation

Cheng Peng
Washington University in St. Louis

WASHINGTON UNIVERSITY IN ST. LOUIS

James McKelvey School of Engineering
Department of Mechanical Engineering & Material Science

Dissertation Examination Committee:
Dr. Ramesh Agarwal, Chair
Dr. Swami Karunamoorthy
Dr. David Peters

Development of a One-Equation Turbulence Model Based on $k-\epsilon$ Closure and its Extension for Computing Transitional Flows by Including an Intermittency Transport Equation

by
Cheng Peng

A dissertation presented to the James McKelvey School of Engineering
of Washington University in St. Louis
in partial fulfillment of the requirements for the degree of
Master of Science

May 2019
St. Louis, Missouri

Table of Contents

List of Figures

List of Tables

Nomenclature

CFD	=	Computational Fluid Dynamics
Re	=	Reynolds number, $\rho u_\infty c/\mu$
Re_v	=	Local vorticity Reynolds number
$Re_{\theta c}$	=	Critical momentum thickness Reynolds number
u	=	x-component of velocity
v	=	y-component of velocity
l	=	Characteristics length
ρ	=	Density
μ	=	Molecular dynamic viscosity
γ	=	Intermittency
$\lambda_{\theta L}$	=	Local pressure gradient parameter
F_{PG}	=	Pressure gradient function
Tu_L	=	Local turbulence intensity
ν	=	Molecular kinematic viscosity
C_f	=	Skin friction coefficient
C_p	=	Pressure coefficient
c	=	Hump length
DES	=	Detached-Eddy Simulation
H	=	Backward facing step height, diffuser inlet height
h	=	Periodic hill height

LES	=	Large Eddy Simulation
L_R	=	Turbulence length scale of KEEB model
M	=	Mach number
P_R	=	Transport variable of elliptic blending equation
RANS	=	Reynolds-Averaged Navier-Stokes
S	=	Strain rate magnitude
SA	=	Spalart-Allmaras
$\widetilde{\nu_t}$	=	Eddy viscosity
κ	=	Von Karman constant
k	=	Turbulent kinetic energy
ϵ	=	Turbulent dissipation
σ	=	Prandtl number
σ_k	=	Turbulent Prandtl number for kinetic energy

Acknowledgments

I would like to offer my special thanks to Dr. Agarwal, my research advisor, for his professional guidance, enthusiastic encouragement and helpful critiques of my research work.

I would also like to thank Dr. Karunamoorthy and Dr. Peters, for serving on my thesis committee and their helpful advice.

I am grateful to my friends in the CFD lab. Thanks to their help and suggestions which assisted a lot in my work.

I would also like to thank my parents whose love and guidance are always with me in whatever I pursue.

Cheng Peng

Washington University in St. Louis

April. 2019

Chapter 1: Introduction

1.1 Background and Motivation

Computational Fluid Dynamics (CFD) has now become an essential tool for engineers for the analysis complex fluid systems in industry, such as aerodynamic design of vehicles of air and ground, turbo machinery design or simulation of blood flow, etc. The CFD codes for simulating flow fields are based on the mathematic models to predict the flow properties. Therefore, it is very important and meaningful to develop an accurate and efficient physical model for computing the flow fields of industrial devices/ products. Turbulent flows are hard to predict because of their feature that the fluid velocity field varies irregularly, almost chaotically in both position and time [1]. Direct numerical simulation (DNS) is an approach to simulate turbulent flows by solving directly the continuity and Navier-Stokes equations without any approximation; however it has extremely high computational cost and at present it is only possible to compute flow in simple geometries at low or moderate Reynolds numbers. Large-eddy simulation (LES) is another approach used for computing turbulent flows. Compared to DNS, it is more efficient since it requires modeling of only small-scale eddies in the boundary layers [1]. Time-averaged Navier-Stokes equation are currently the most wieldy equations for solving turbulent flows in industrial applications. RANS equations solve for the mean velocity field; however, they contain unknown turbulent stresses called Reynolds stresses which need to be modeled; This is the so-called closure problem for RANS equations and requires

turbulence models for calculating the Reynolds stresses. The object of this thesis is to develop accurate and efficient turbulence models for the solution of RANS equations.

1.2 Outline

The focus of this thesis is to develop a new one-equation turbulence model based on two-equation $k-\epsilon$ closure and a new transition model by integrating an intermittency transport equation with one-equation $k-\epsilon$ model. The performance of both the turbulence and transition models is evaluated by computing several benchmark test cases and the computational results from the new developed models are compared with the available experimental data or LES or DNS computations. The major accomplishments are described below:

Chapter 2: Turbulence Modeling: In this chapter, a brief introduction to turbulence modeling is given. Then main approaches for calculating turbulent flows, namely the Reynolds-Averaged Navier-Stokes (RANS) equations, Large-Eddy Simulation (LES) and Direct Numerical Simulations (DNS) are described

Chapter 3: The One-Equation $k-\epsilon$ Turbulence model: This chapter reviews formulations of one-equation SA model, two-equation $k-\epsilon$ turbulence model and one-equation $k-\epsilon$ turbulence model (KE model).

Chapter 4: The Elliptic Blending: This chapter describes the integration of the elliptic blending (elliptic relaxation) equation with the one-equation $k-\epsilon$ turbulence model (KE model). The new developed model which is designated as KEEB model as well as the KE model are tested for several benchmark cases to show

substantial improvement in computing for wall bounded mildly separated flows using the KEEB model.

Chapter 5: Development of a Transition Model: Development and implementation of the intermittency equation γ with the one-equation $k-\epsilon$ turbulence model is described in this chapter, which results in the $k\epsilon-\gamma$ transition model. The new transition model is validated by computing the benchmark cases: the ERCOFTAC T3 flat plate series, the S809 airfoil, the Aerospatiale-A airfoil, and the NLR-7301 two-element airfoil.

Chapter 6: Summary and Future Work: This chapter provides a summary of the work accomplished in this thesis, including modeling and testing of the KEEB turbulence model and $k\epsilon-\gamma$ transition model. The future work describes the proposed approach for the development of one-equation $k-\epsilon$ turbulence model based algebraic laminar-turbulent transition model.

Chapter 2: Turbulence Modeling

2.1 Laminar and Turbulent Flow

Laminar flow and turbulent flow are two widely used terms to describe the nature of a flow field. The adjacent fluid layers of the laminar flow, which tend to occur at low velocities, do not mix with each other and slide parallel to one another. Because of the orderly motion of the particles of the fluid, the shear stress in laminar flow only depends on the velocity of the fluid. In contrast, the turbulent flow, which is a result of extensive momentum and energy transfer in various regions of the fluid flow, undergoes chaotic fluctuation and mixing. The change from laminar flow to turbulent flow can be characterized by a dimensionless constant, which is called the Reynolds number. The expression of Reynolds number is given as:

$$Re = \frac{\rho u l}{\mu} = \frac{u l}{\nu} \tag{2.1}$$

2.2 Turbulence Modeling

2.2.1 Introduction

Turbulence flows are very common in our daily life, e.g. smoke from a chimney, flow over an aircraft wing, or intense oceanic currents, etc. Because of the effects of turbulent flows on our daily life and in many engineering applications, it is important to accurately predict the turbulent flows. Turbulence modelling is one way to predict properties of turbulent flows by developing turbulence models which are needed in the solution of Reynolds-Averaged Navier-Stokes (RANS) equations for analyzing

turbulent flows. In past several decades, several approaches have been developed for solving turbulent flows. They are known as the Direct Numerical Simulation (DNS), Reynolds-Averaged Navier-Stokes (RANS) equations and Large-Eddy Simulations (LES). The focus of this thesis is primarily on turbulence modeling required for the solution of RANS equations.

2.2.2 Reynolds-Averaged Navier-Stokes (RANS) Equations

Reynold-Averaged Navier-Stokes (RANS) equations model is the oldest model based on time-averaging of the Navier-Stokes equation to mathematically predict the turbulence flow behavior. The averaging of Navier-Stokes equations results in "turbulent stresses" or "Reynolds Stresses" which require modeling using empiricism. RANS equations in conjunction with turbulence models offer the most economic approach for computing turbulent flows and are widely used in almost all engineering applications and they typically provide the level of accuracy required.

2.2.3 Large-Eddy Simulation (LES)

Large-Eddy simulation was initially proposed by Joseph Smagorinsky in 1963 to simulate atmospheric air currents [2]. A filtering operation is applied to separate velocity field into filtered component and residual (or subgrid-scale, SGS) component. The filtered component which represents larger scales of motion is computed directly by solving the Navier-Stokes equations. In contrast, the residual (or SGS) component, representing the smaller scales of motion, is calculated by a turbulence model. Compared to the DNS, which solves the Navier-Stokes equations for the whole

turbulent flow fields without any approximation, LES lies between RANS Modeling and DNS for both accuracy and computational expense aspects.

2.2.4 Direct Numerical Simulation (DNS)

Direct Numerical Simulation (DNS) is a simulation in computational fluid dynamics in which the Navier-Stokes equations are numerically solved without any turbulence model. Because of the high computational cost of DNS, this method is currently able to calculate flows with low to moderate Reynolds number for some practical geometries, such as flow in a channel or over a flat plate. Among these three methods, DNS is the most accurate one to simulate the flow fields.

Chapter 3: The One-Equation k-ϵ Turbulence model

3.1 Introduction

In recent years, a number of one-equation turbulence models have been proposed for the solution of Reynolds-Averaged Navier-Stokes (RANS) equations. Some of these are Menter's one-equation eddy viscosity model based on $k-\epsilon$ model [3], Wray-Agarwal model [4], Rahman-Agarwal-Siikonen (RAS) model [5], and one-equation model based on two-equation k-kL model [6]. One of the most well-known and widely used one-equation model is the Spalart-Allmaras (SA) model [7]. In the category of two-equation models, most well-known models and widely used models are k-ϵ model [8], Wilcox k-ω model [9] and SST $k-\omega$ model [10]. To improve the accuracy, SA model and one- and two-equation models have been revised several times over the years as noted in NASA TMR [11]. Menter [3] considered the standard $k-\epsilon$ model and proposed a one-equation eddy-viscosity model employing some assumptions. Because of close connection with the standard $k-\epsilon$ model, his model has some deficiencies. As a result, compared to the one-equation SA model or the two-equation SST $k-\omega$ model, the one-equation eddy viscosity model based on $k-\epsilon$ model does not perform that well.

3.2 Review of the SA and $k-\epsilon$ Model

3.2.1 Review of the One-Equation SA Model

The Spalart-Allmaras (SA) model is a one-equation model developed for aerodynamic flows, such as transonic flow over airfoils including boundary-layer separation [1]. SA model is computationally simpler than two-equation models, therefore this model is wieldy used in industry. The SA model is given by the following equation:

$$\frac{\partial \tilde{\nu}}{\partial t} + u_j \frac{\partial \tilde{\nu}}{\partial x_j} = c_{b1}(1 - f_{t2})\tilde{S}\tilde{\nu} - \left[c_{w1} f_w - \frac{c_{b1}}{\kappa^2} f_{t2}\right]\left(\frac{\tilde{\nu}}{d}\right)^2 + \frac{1}{\sigma}\left[\frac{\partial}{\partial x_j}\left((\nu + \tilde{\nu})\frac{\partial \tilde{\nu}}{\partial x_j}\right) + c_{b2}\frac{\partial \tilde{\nu}}{\partial x_i}\frac{\partial \tilde{\nu}}{\partial x_i}\right] \quad (3.1)$$

The turbulent eddy viscosity is computed from:

$$\mu_t = \rho \tilde{\nu} \quad (3.2)$$

where

$$f_{v1} = \frac{\chi^3}{\chi^3 + {C_{v1}}^3} \quad (3.3)$$

$$\chi = \frac{\tilde{\nu}}{\nu} \quad (3.4)$$

and ρ is the density, $\nu = \mu/\rho$ is the molecular kinematic viscosity, and μ is the molecular dynamic viscosity. Additional definitions are given by the following equations:

$$S = \Omega + \frac{\tilde{\nu}}{\kappa^2 d^2} f_{v2} \quad (3.5)$$

where $\Omega = \sqrt{2W_{ij}W_{ij}}$ is the magnitude of the vorticity, d is the distance from the field point to the nearest wall, and

$$f_{v2} = 1 - \frac{\chi}{1 + \chi f_{v1}} \qquad f_w = g\left[\frac{1 + c_{w3}^6}{g^6 + c_{w3}^6}\right]^{1/6} \quad (3.6)$$

$$f_{t2} = c_{t3} \exp(-c_{t4}\chi^2) \quad (3.7)$$

3.2.2 Review of the Two-Equation $k-\epsilon$ Model

The two-equation $k-\epsilon$ model is the most wieldy used turbulence model to compute flow characteristics of turbulent flows. This model consists of two transport equations which are solved for two turbulence quantities, k and ϵ. The two transport equations are described as:

$$\frac{Dk}{Dt} = \widetilde{\nu_t}\left(\frac{\partial u}{\partial y}\right)^2 - \epsilon + \frac{\partial}{\partial y}\left(\frac{\widetilde{\nu_t}}{\sigma_k}\frac{\partial}{\partial y}(k)\right) \tag{3.8}$$

$$\frac{D\epsilon}{Dt} = c_{\epsilon 1}\frac{\epsilon}{k}\widetilde{\nu_t}\left(\frac{\partial u}{\partial y}\right)^2 - c_{\epsilon 2}\frac{\epsilon^2}{k} + \frac{\partial}{\partial y}\left(\frac{\widetilde{\nu_t}}{\sigma_\epsilon}\frac{\partial}{\partial y}(\epsilon)\right) \tag{3.9}$$

The eddy viscosity is given by:

$$\widetilde{\nu_t} = c_\mu \frac{k^2}{\epsilon} \tag{3.10}$$

The five empirical constants in this model are:

$$c_\mu = 0.09 \quad c_{\epsilon 1} = 1.44 \quad c_{\epsilon 2} = 1.92 \quad \sigma_k = 1.0 \quad \sigma_\epsilon = 1.3$$

3.3 One-Equation $k-\epsilon$ Turbulence Model

One-equation eddy viscosity model based on the two-equation $k-\epsilon$ model is described in this section. The one equation model is derived from the standard $k-\epsilon$ closure using the definition of the eddy viscosity $\widetilde{\nu_t} = C_\mu \frac{k^2}{\epsilon}$ [3]. In order to arrive at a one-equation model, we follow Baldwin and Barth and express the time derivative of the eddy viscosity by the time derivatives of k and ϵ:

$$\frac{D\widetilde{\nu_t}}{Dt} = C_\mu\left(2\frac{k}{\epsilon}\frac{Dk}{Dt} - \frac{k^2}{\epsilon^2}\frac{D\epsilon}{Dt}\right) \tag{3.11}$$

Replacing the total derivatives of k and ϵ on the right-hand side by the ride-hand side of Eq. (3.8) and Eq. (3.9) gives a single transport equation for the eddy viscosity.

In order to close the equation, two additional relations have to be provided. The first one is definition of the eddy viscosity, which is given by:

$$\epsilon = C_\mu \frac{k^2}{\widetilde{\nu_t}} \tag{3.12}$$

A second equation is a relation readily available that relates the turbulent kinetic energy and eddy viscosity, which has been confirmed for a large number of experimental boundary layer data:

$$\widetilde{\nu_t} \left|\frac{\partial u}{\partial y}\right| = a_1 k \tag{3.13}$$

The one-equation model can be derived by straightforward substitution and the final form of the one-equation model can be written as:

$$\frac{D\widetilde{\nu_t}}{Dt} = c_1 D_1 \widetilde{\nu_t} S - c_2 E_{1e} + \frac{\partial}{\partial x_j}\left(\left(\nu + \frac{\widetilde{\nu_t}}{\sigma}\right)\frac{\partial}{\partial x_j}(\widetilde{\nu_t})\right) \tag{3.14}$$

$$\nu_t = D_2 \widetilde{\nu_t} \tag{3.15}$$

In Eq. (3.14) and Eq. (3.15), two damping functions D_1 and D_2 are given by:

$$D_1 = \frac{\nu_t + \nu}{\widetilde{\nu_t} + \nu} \tag{3.16}$$

$$D_2 = 1 - e^{-\left(\frac{\widetilde{\nu_t}}{\kappa \nu A^+}\right)^2} \tag{3.17}$$

The strain rate magnitude is defined as:

$$S = \sqrt{U_{i,j}\left(U_{i,j} + U_{j,i}\right)} \tag{3.18}$$

The term involving the inverse of von Karman length-scale is given as:

$$E_{k-\epsilon} = \widetilde{\nu_t}^2 \left(\frac{1}{L_{VK}}\right)^2 = \widetilde{\nu_t}^2 \left(\frac{\frac{\partial s}{\partial x_j}\frac{\partial s}{\partial x_j}}{s^2}\right) \tag{3.19}$$

$$E_{1e} = c_3 E_{BB} tanh\left(\frac{E_{k-\epsilon}}{c_3 E_{BB}}\right) \tag{3.20}$$

where the Baldwin-Barth destruction term is defined as:

$$E_{BB} = \frac{\partial \widetilde{\nu_t}}{\partial x_j} \cdot \frac{\partial \widetilde{\nu_t}}{\partial x_j} \tag{3.21}$$

The model constants used in one-equation eddy viscosity model in Eq. (3.14) are given as: $c_1 = 0.144$, $c_2 = 1.86$, $c_3 = 7$, $\sigma = 1$, $\kappa = 0.41$, $A^+ = 13$.

Chapter 4: The Elliptic Blending

4.1 Introduction

Elliptic blending can successfully address the problem of log-layer mismatch in the turbulent boundary layer. The wall blocking is governed by an elliptic partial differential equation which introduces near wall anisotropy [12]. The original one-equation $k-\epsilon$ model is modified and combined with an elliptic relaxation. The new model is tested on several benchmark test cases selected from NASA TMR [11]. The results from the new one-equation model $k-\epsilon$ with elliptic blending show better agreement with DNS data in capturing the velocity profile in the entire boundary layer including the sub-layer, buffer layer and log layer compared to the model without elliptic blending.

4.2 Derivation of Elliptic Blending for One-Equation $k-\epsilon$ Turbulence model

Based on the work of Han et al. [12], it can be concluded that an elliptic relaxation applied to a turbulence model can capture the anisotropic low Reynolds number near wall effects more accurately. Following the form of the elliptic blending in WA2018EB model [12], elliptic blending is added into the present one-equation $k-\epsilon$ model considered in this paper. The equation for elliptic blending can be expressed as:

$$-L_R^2\nabla^2 P_R + P_R = \widetilde{\nu_t}S \tag{4.1}$$

where P_R is a production term. The coupled one-equation $k-\epsilon$ model with elliptic blending can be expressed as:

$$\frac{D\widetilde{\nu_t}}{Dt} = c_1 D_1 \widetilde{\nu_t} S - c_2 E_{1e} + \frac{\partial}{\partial x_j}\left(\left(\nu + \frac{\widetilde{\nu_t}}{\sigma}\right)\frac{\partial}{\partial x_j}(\widetilde{\nu_t})\right) + P_R - \widetilde{\nu_t} S \tag{4.2}$$

$$\nu_t = D_2 \widetilde{\nu_t} \tag{4.3}$$

$$-L_R^2 \nabla^2 P_R + P_R = \widetilde{\nu_t} S \tag{4.4}$$

$$L_R^2 = \frac{max(C_{3k\omega}\widetilde{\nu_t}, C_l \upsilon)}{S + \frac{C_l \upsilon}{{L_{ref}}^2}} \tag{4.5}$$

$$C_l = 4.0 + \sqrt{\chi} \tag{4.6}$$

In Eq. (4.5) for L_R and C_l are used to correct for the free stream behavior of L_R and $L_{ref} = 1$ is the reference length scale. The calibrated coefficients used in the one-equation $k - \epsilon$ model with elliptic blending are as follows: $c_1 = 0.308$, $c_2 = 3.097$, $c_3 = 7$, $\sigma = 1$, $\kappa = 0.41$, $A^+ = 8.36$, $C_{3kw} = 0.539$.

4.3 Validation Cases

This section shows the comparison of results computed by one-equation model based on k-ϵ closure (designated as KE model) and the one-equation model with elliptic blending （designated as KEEB model). Several benchmark cases are tested to show the performance and accuracy of these two models (KE and KEEB). The results are compared with the DNS data or experimental results for each case to compare the KE and KEEB models. All the results are computed by using the open source CFD software OpenFOAM.

4.3.1 Zero Pressure Gradient Boundary-Layer Flow past a Flat Plate

Flow past a flat plate is a basic case used to verify the accuracy of any turbulence model. Figure 4.1 shows the computational setup and boundary conditions from

NASA TMR [11]. Figure 4.2 shows the computational result for wall skin-friction coefficient C_f vs. Reynolds number Re based on length in x direction (Re_x) and their comparison with experimental data. Re_x is defined as:

$$Re_x = \frac{\rho_\infty U_\infty x}{\mu_\infty} \tag{4.7}$$

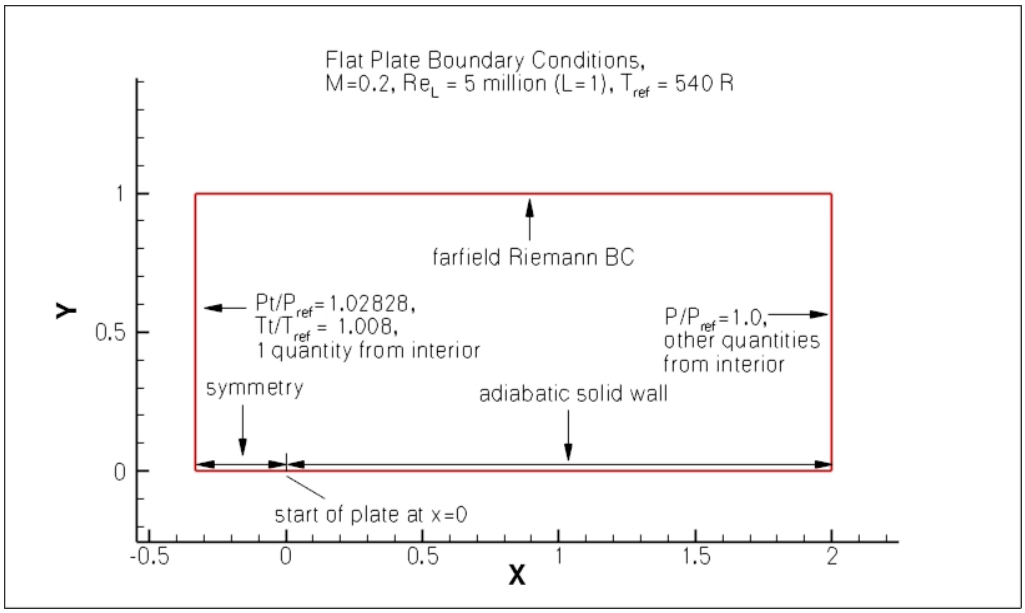

Figure 4. 1: Flat plate geometry and boundary conditions [11].

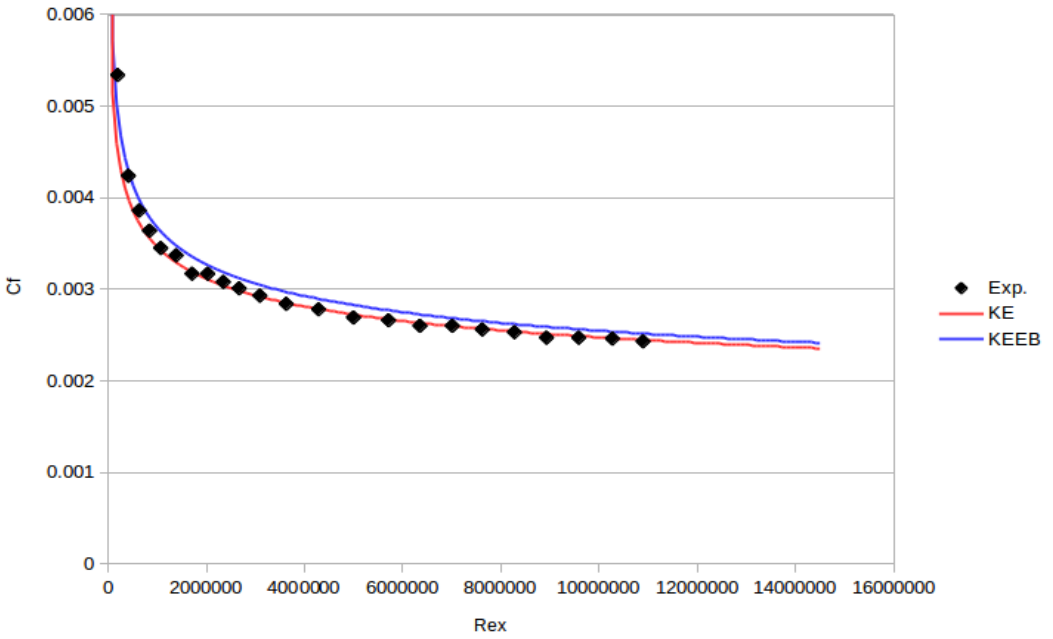

Figure 4. 2: Comparison of computed C_f on the flat plate with the experimental data.

Figure 4.2 shows that the one-equation KE model has slightly better accuracy compared to the KEEB model. The KE model completely matches the experimental data. However, the errors between the results computed by KEEB model and experimental data are quite acceptable when considering the significant improvement of the results of KEEB model in the 2D channel case as shown in the next section. The other more complex computations also show the superiority of KEEB model over KE model.

4.3.2 Flow in a 2D Channel at Different Reynolds Numbers

Fully developed turbulent flow in a channel is another basic test case frequently used to assess the accuracy of various turbulence models. Figures 4.3 - 4.12 show results in a simple channel flow at several friction Reynolds number ranging from Re_τ = 182 to 5200 and are compared with DNS data by Lee and Moser [13].

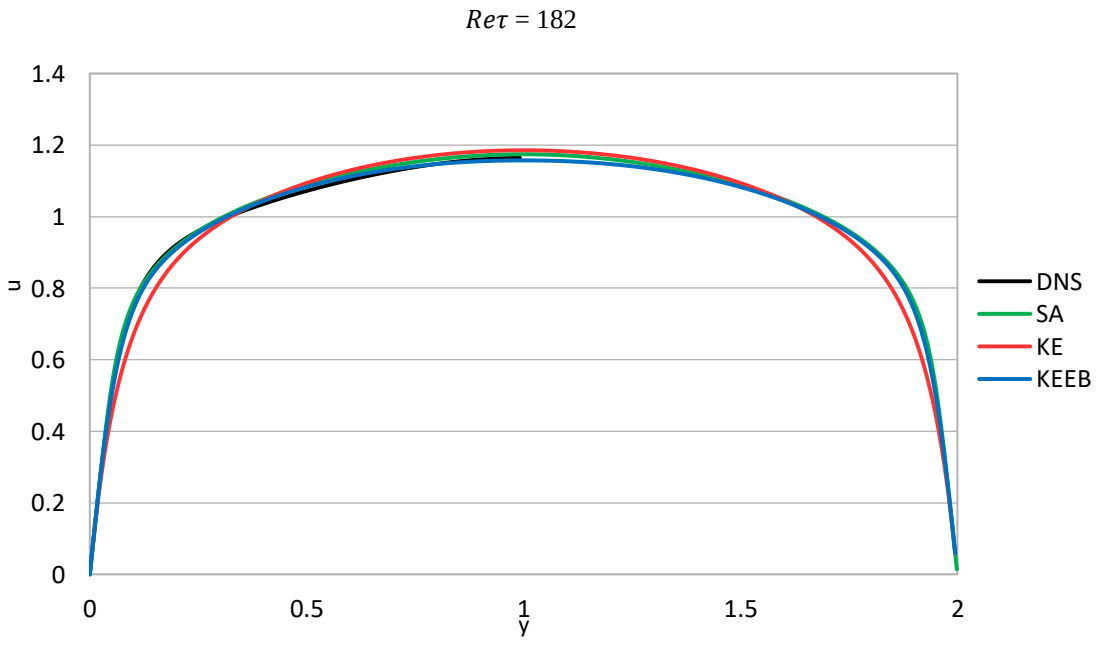

Figure 4. 3: Comparison of the velocity profile in turbulent channel flow at Re_τ = 182.

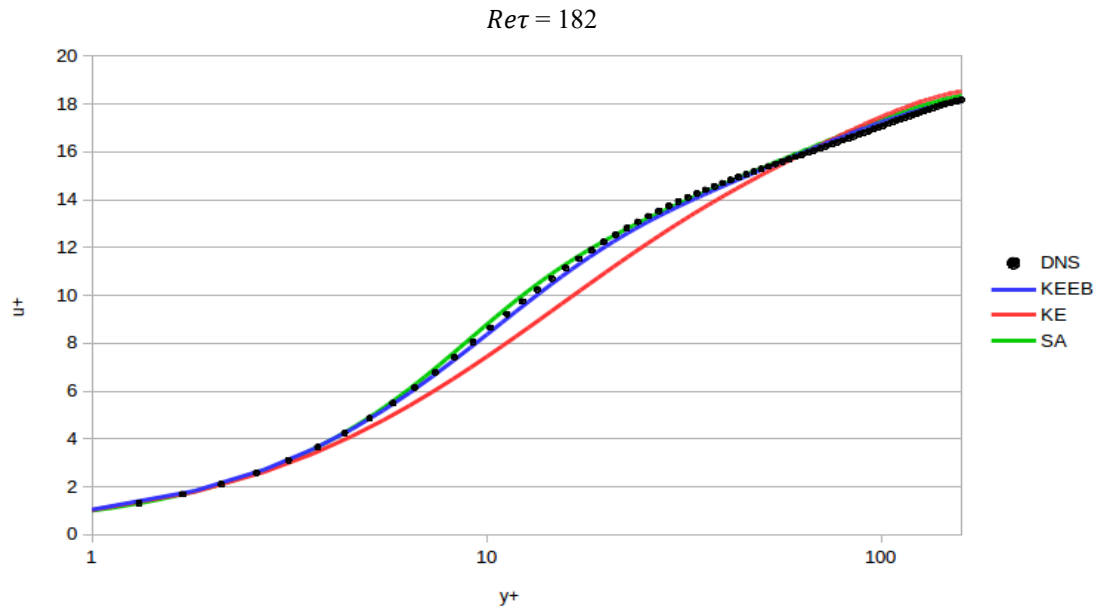

Figure 4. 4: Comparison of velocity profile in log layer for turbulent flow in a channel at Re_τ = 182.

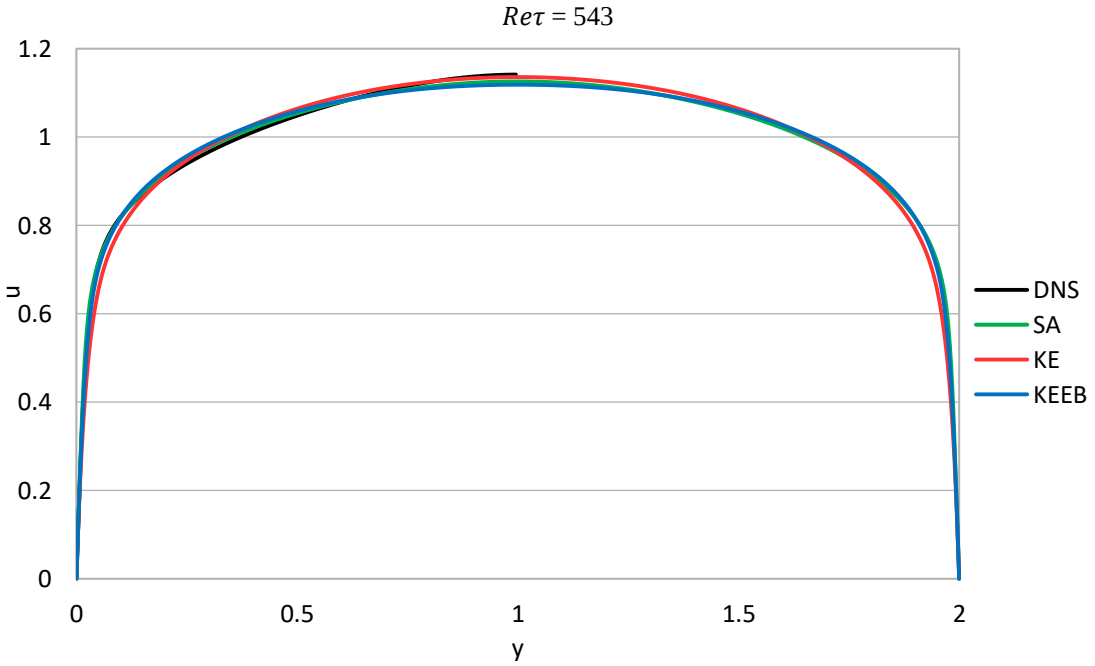

Figure 4. 5: Comparison of velocity profile in turbulent channel flow at Re_τ = 543.

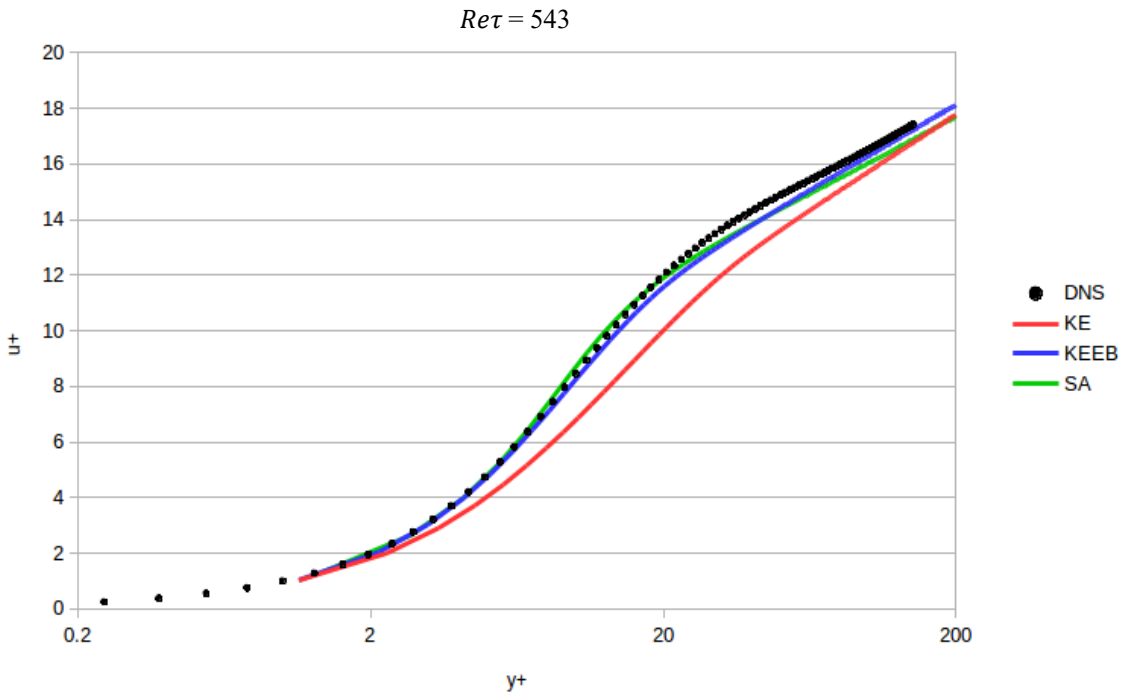

Figure 4. 6: Comparison of velocity profile in log layer in turbulent channel at Re_τ = 543.

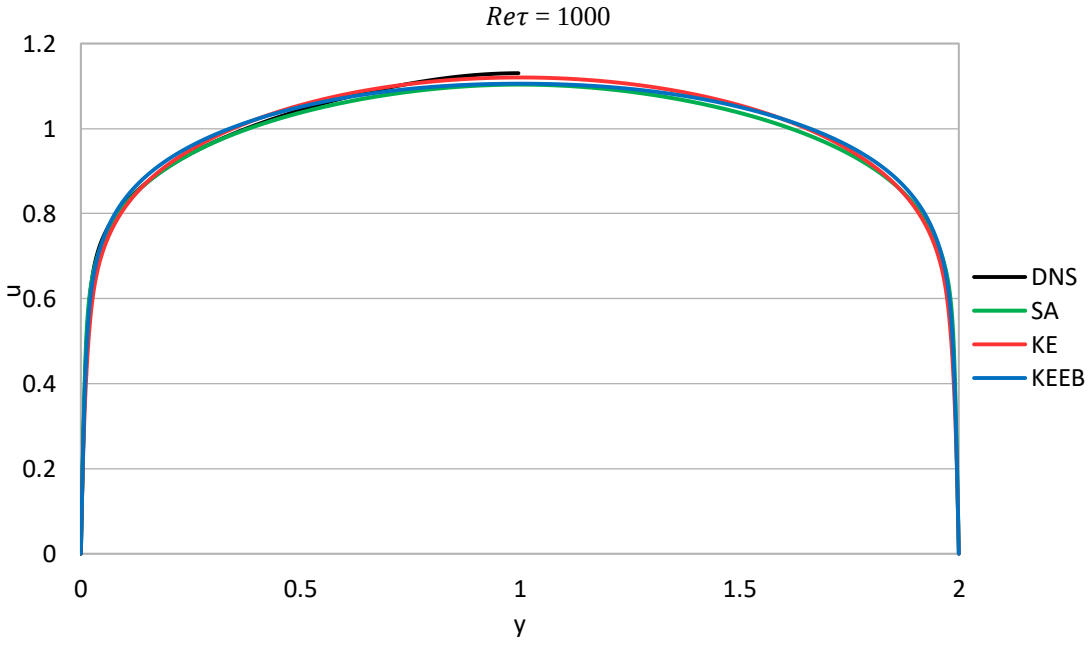

Figure 4. 7: Comparison of velocity profile in turbulent channel flow at Re_τ = 1000.

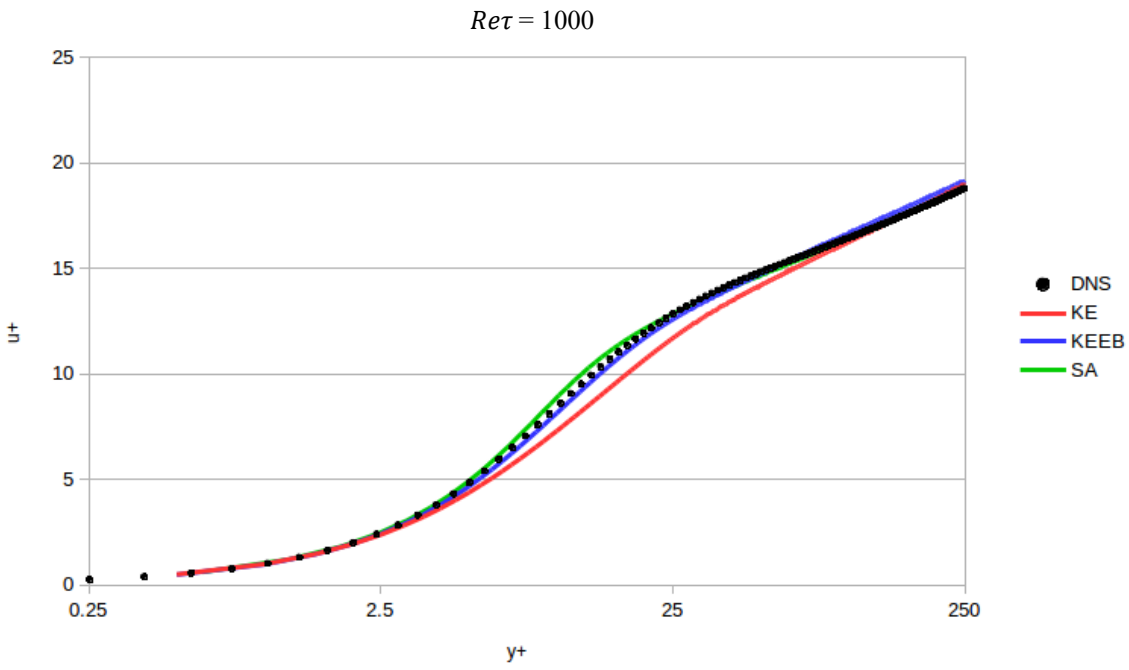

Figure 4. 8: Comparison of velocity profile in log layer in turbulent channel at Re_τ = 1000.

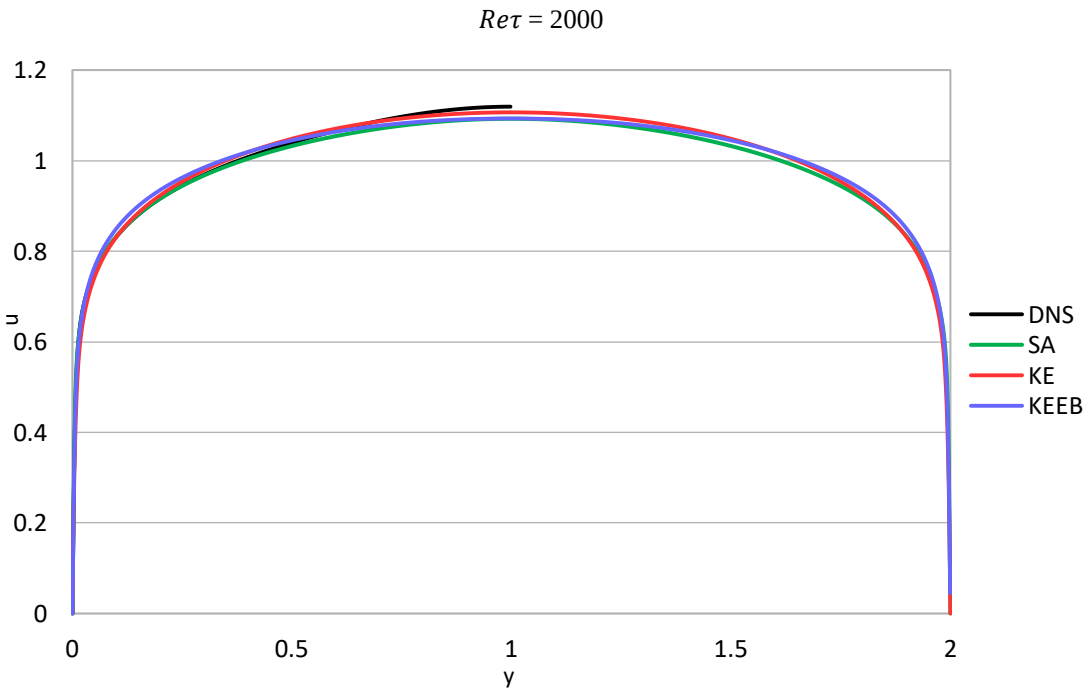

Figure 4. 9: Comparison of velocity profile in turbulent channel flow at Re_τ = 2000.

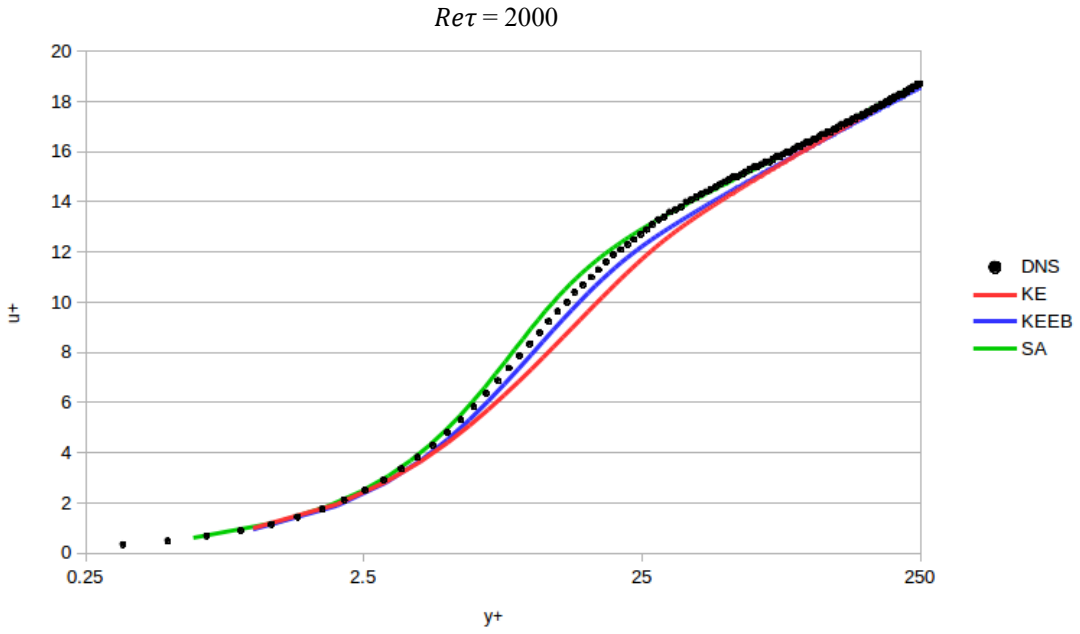

Figure 4. 10: Comparison of velocity profile in log layer in turbulent channel at Re_τ = 2000.

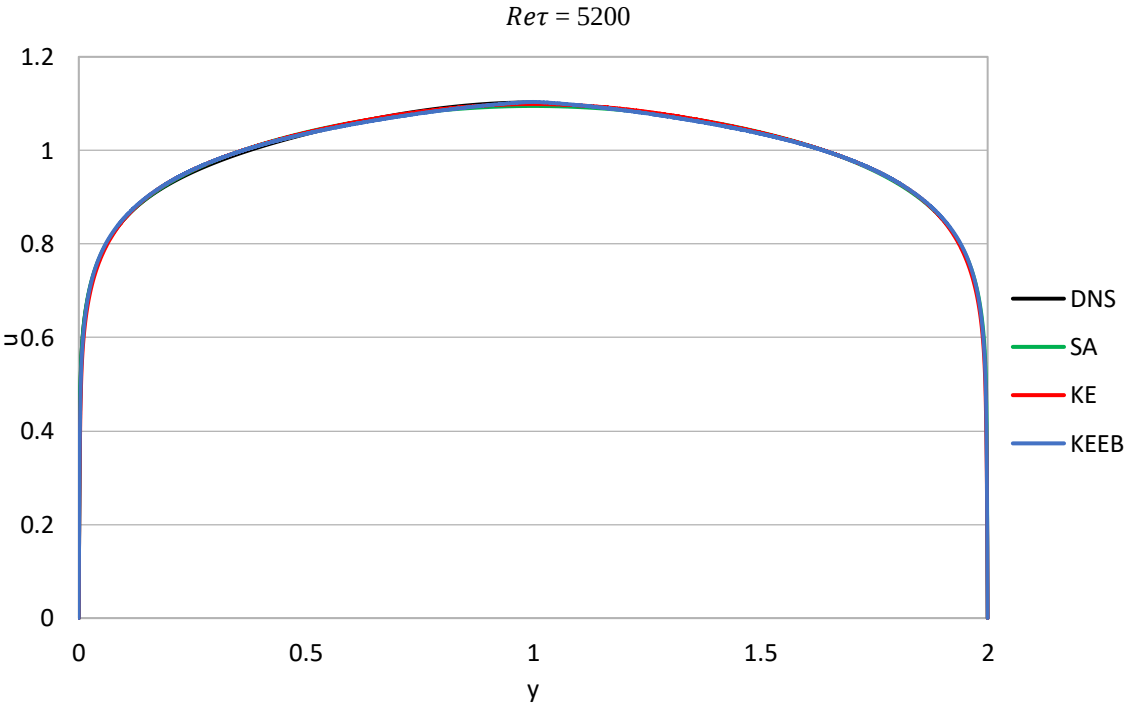

Figure 4. 11: Comparison of velocity profile in turbulent channel flow at Re_τ = 5200.

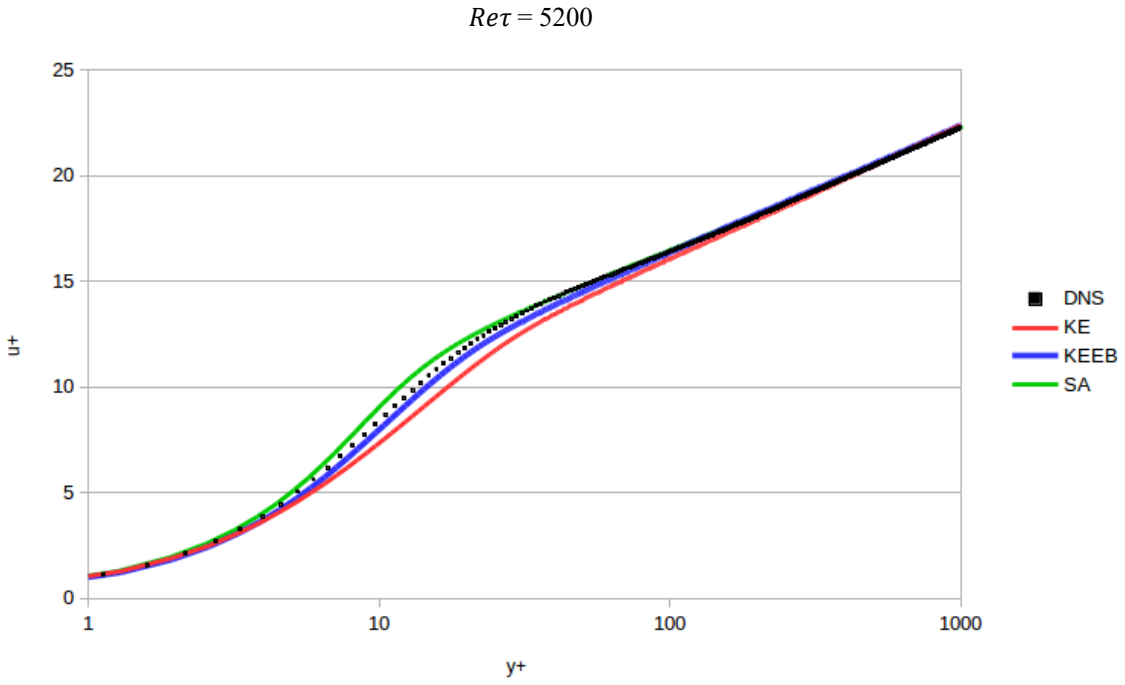

Figure 4. 12: Comparison of velocity profile in log layer in turbulent channel flow at Re_τ = 5200.

From Figures 4.3 - 4.12, it can be seen that both KE model and KEEB model can predict the fully developed turbulent channel flow velocity profiles quite well. However, when Re_τ = 182, the results from KEEB model are in better agreement with DNS data compared to the KE model.

For the velocity profiles in the sublayer region, both models agree with the DNS data very well. However, in the buffer layer and log layer region, there is a large mismatch between the results from KE model and the DNS data. KEEB model shows significant improvement compared to the KE model in this region close to the channel wall, which demonstrates that the elliptic blending is beneficial in improving the performance of a turbulence model in buffer layer and log layer region. Overall, it can be concluded that KEEB model improves the results in computing wall bounded turbulent flows.

4.3.3 Flow over NASA Wall-Mounted Hump

The configuration and boundary conditions of wall-mounted hump are shown in Figure 4.13. The Mach number of the freestream is 0.1 and Reynolds number based on hump chord length is $\mathrm{Re_c} = 936{,}000$[11]. This test case is a widely used and challenging case for testing the accuracy of turbulence models.

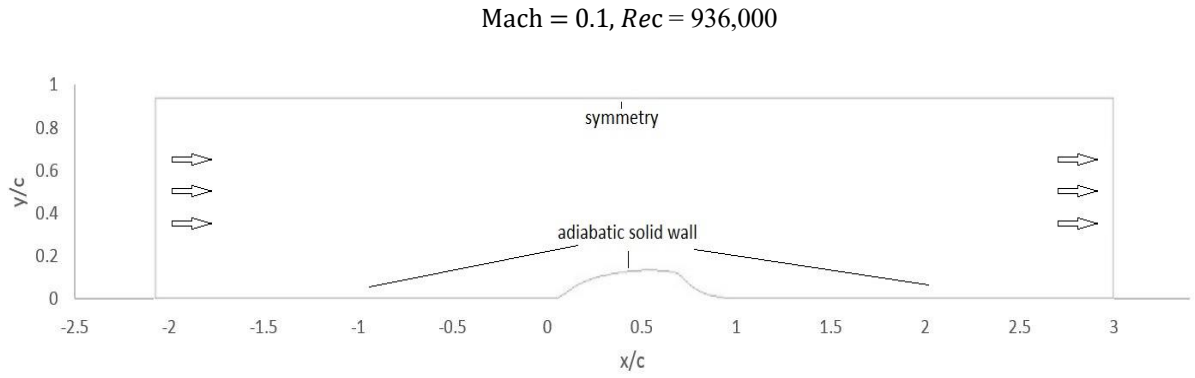

Figure 4. 13: Wall-mounted hump configuration and boundary conditions.

Figure 4.14 shows the comparison of pressure coefficient computed by KEEB model, KE model and SA model with the experimental data. Figure 4.15 shows the comparison of skin-friction distribution computed by the same models with the experimental data. It is can be seen that the results obtained by KEEB model have better agreement with the experimental data than the results calculated by KE model. It can also be concluded that KEEB model performs as good as the SA model in this case.

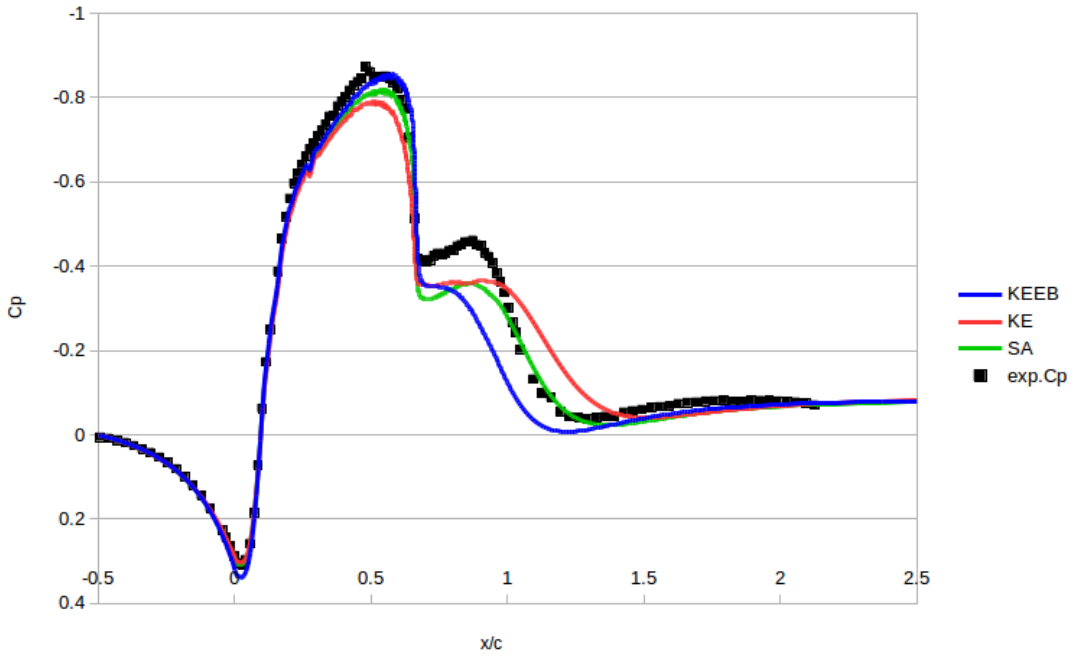

Figure 4. 14: Comparison of pressure distribution on the surface of the hump.

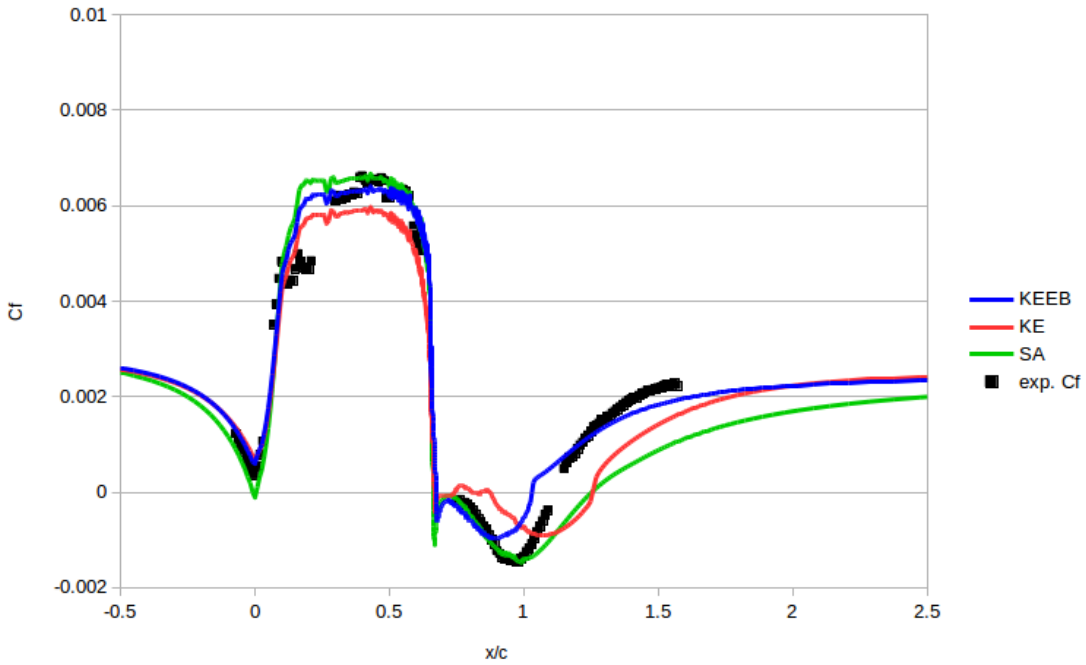

Figure 4. 15: Comparison of Skin-Friction distribution on the surface of the hump.

4.3.4 Flow over a Periodic Hill

Flow over a periodic hill is also a widely used benchmark test case for turbulence model validation for wall bounded flows with separation. Details of this model can be found in the European Research Community on Flow, Turbulence and Combustion (ERCOFTAC) database [15]. The hill has a height h = 28mm and the Reynolds number based on hill height h is 10,595. Simulation results from KEEB model are compared to KE and SA models and the LES results computed by Frohlich et al. [16], which are provided in the ERCOFTAC database and NASA Langley Research Center Turbulence Modeling Resource [11]. The comparison of the skin friction distribution on the hill is shown in Figure 4.16. Though none of the models match the LES results very well, KEEB model performs slightly better than the KE model for the region from x/h = 6.0 to 7.5. The comparison of the pressure distribution on the hill and top wall is shown in Figure 4.17 and Figure 4.18 respectively. KEEB model has the best agreement with the LES solution compared to KE and SA models, although none of the models can compute this flow satisfactorily.

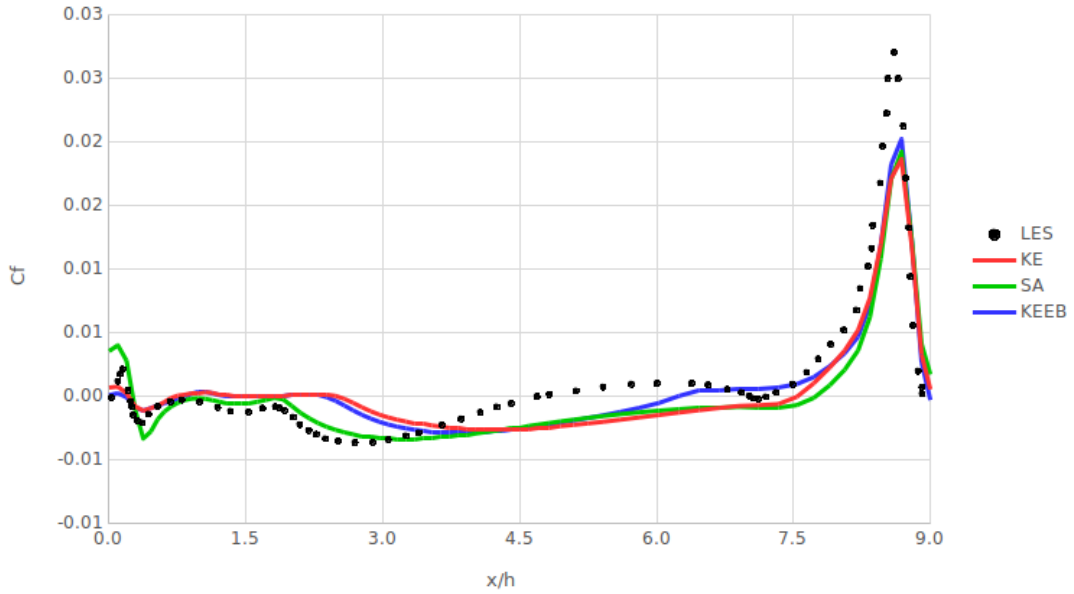

Figure 4. 16: Comparison of skin friction coefficient distribution on the periodic hill.

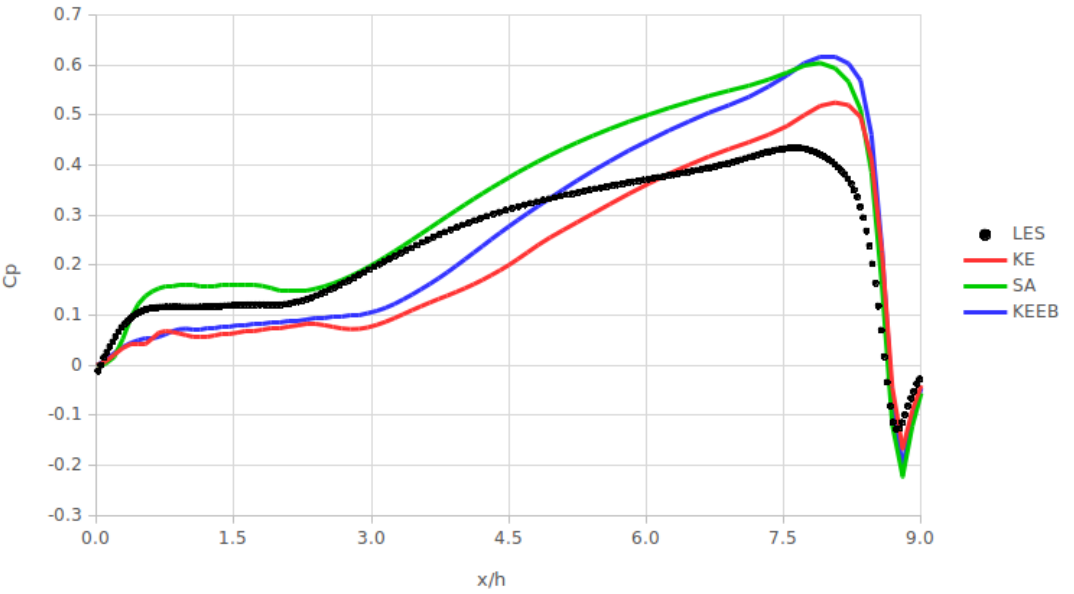

Figure 4. 17: Comparison of pressure coefficient distribution on the periodic hill.

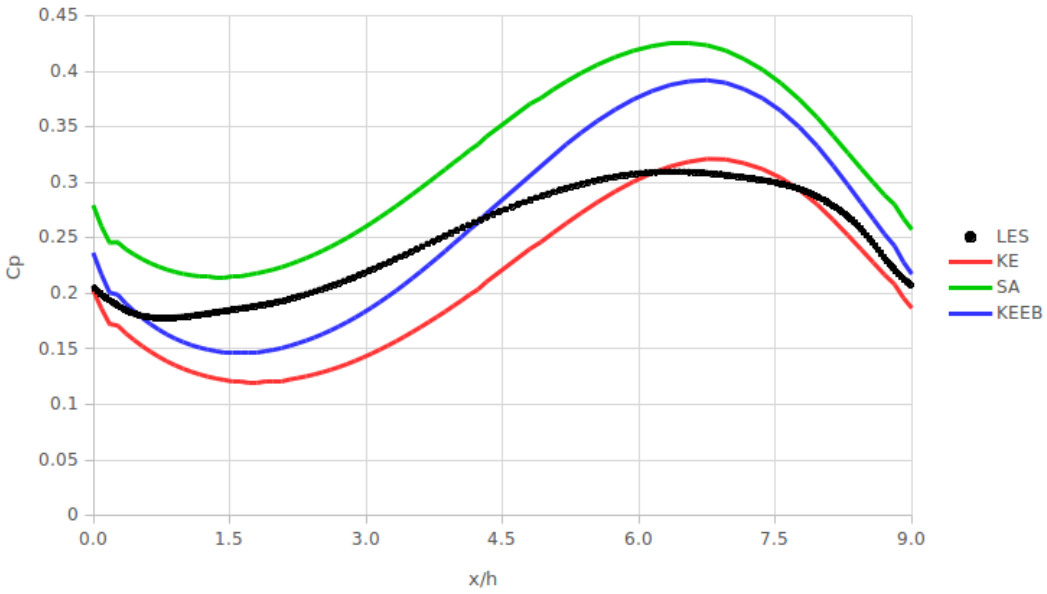

Figure 4. 18: Comparison of pressure coefficient distribution on the top surface of the periodic hill.

4.3.5 Flow in an Asymmetric Plane Diffuser

The geometry of an asymmetric plane diffuser is shown in Figure 4.19. The Mach number of the inflow is 0.06 and the Reynolds number based on H is $Re_H = 20{,}000$ [17]. KEEB model results are compared to the results from KE and SA models and experimental data for the skin friction distribution on the top wall in Figure 4.20 and on the bottom wall in Figure 4.21. As shown in Figure 4.20, computations from KEEB and KE models show good agreement with the experimental data for the skin friction on the top wall of the diffuser. For the bottom wall of the diffuser, as shown in Figure 4.21, the computed skin friction results from KEEB model outperform those obtained from the KE model; however, SA model shows the best agreement with the experimental data in this case. Overall, none of the models computes the skin friction satisfactorily on both the walls.

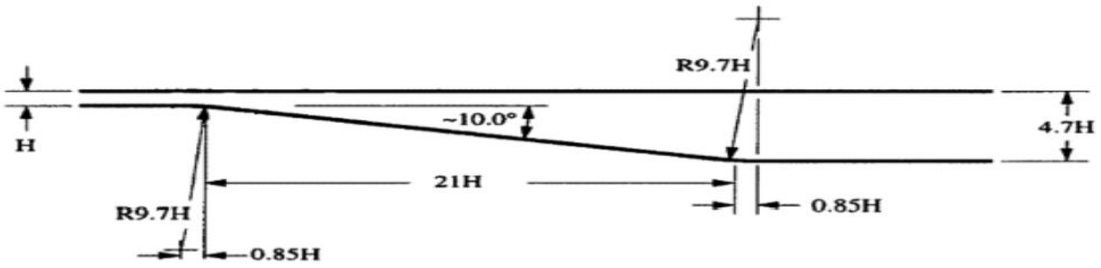

Figure 4. 19: Geometry of the asymmetric plane diffuser [14].

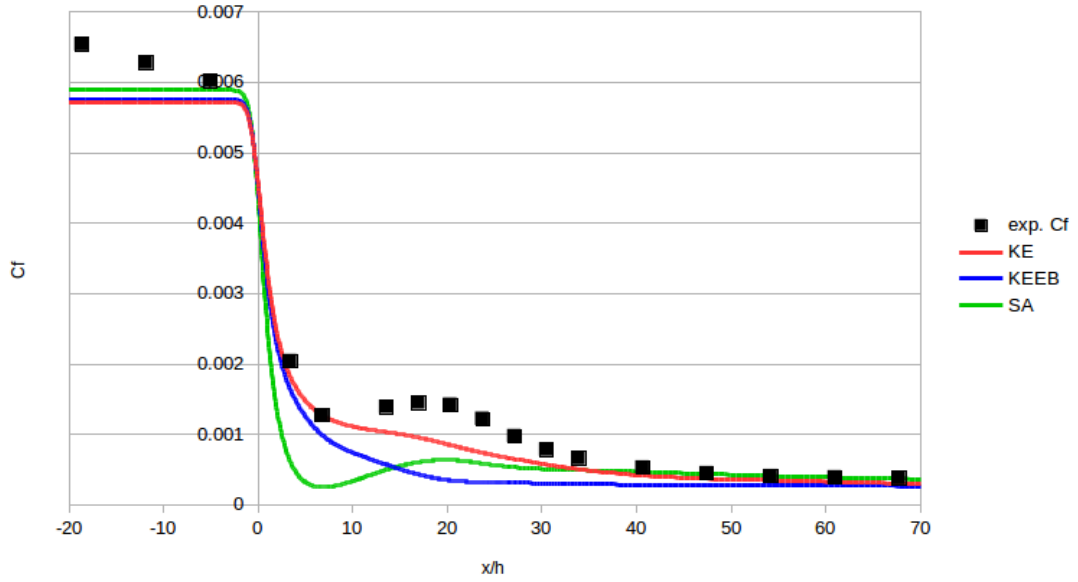

Figure 4. 20: Comparison of skin-friction distribution on top wall of the diffuser.

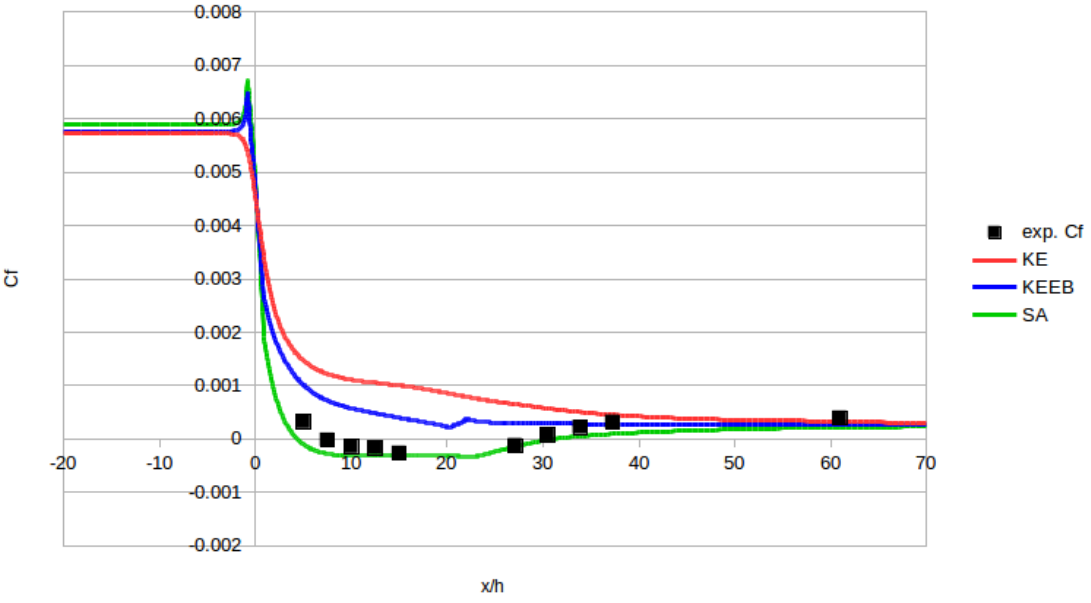

Figure 4. 21: Comparison of skin-Friction distribution on the bottom wall of the diffuser.

4.3.6 Flow over a Backward Facing Step

In this case, a turbulent boundary layer encounters a sudden back step, causing flow separation. The flow then reattaches and recovers downstream of the step [11]. Figure 4.22 shows the configuration and boundary conditions of backward facing step. The Reynolds number based on step height H is $Re_H = 36{,}000$ and the Mach number at point (x/H = -4) is 0.128. This is a widely-tested case for turbulence modeling validation.

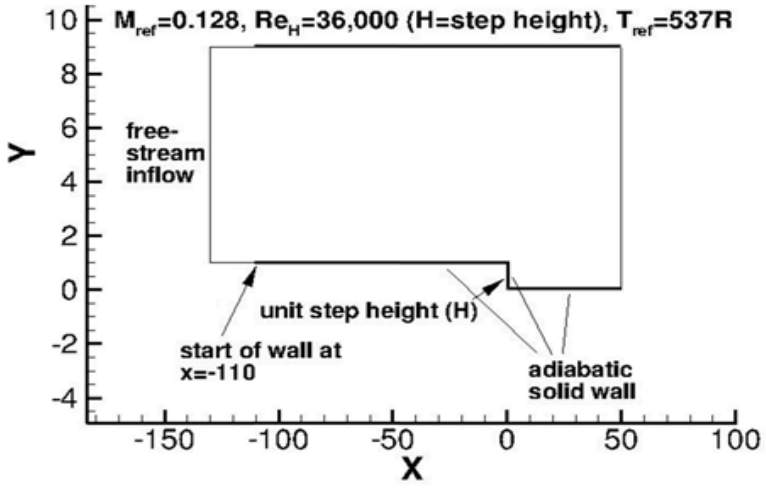

Figure 4. 22: Backward facing step configuration and boundary conditions [11].

Figures 4.23 and 4.24 show the pressure distribution and skin friction coefficient respectively computed by the KEEB and KE model and their comparison with the experimental data [14]. Both the pressure distribution and skin friction coefficient predicted by the KEEB model generally match the experimental data; however, the overall performance of KEEB model is not as good as that of KE model and SA model and KE model has the best match with the experimental data,

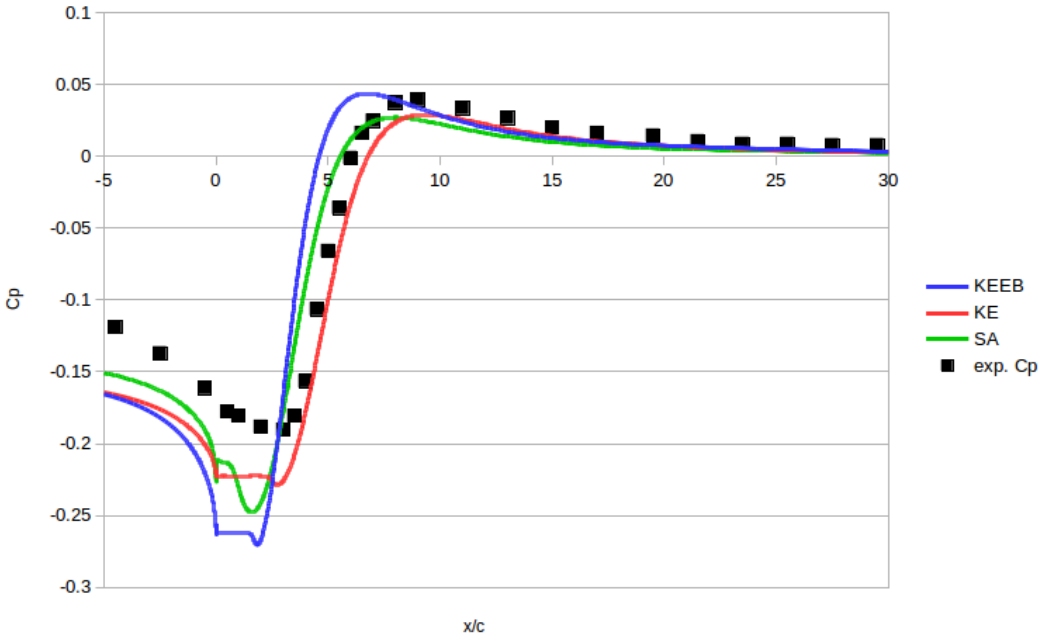

Figure 4. 23: Comparison of pressure distribution on the surface of the backward facing step.

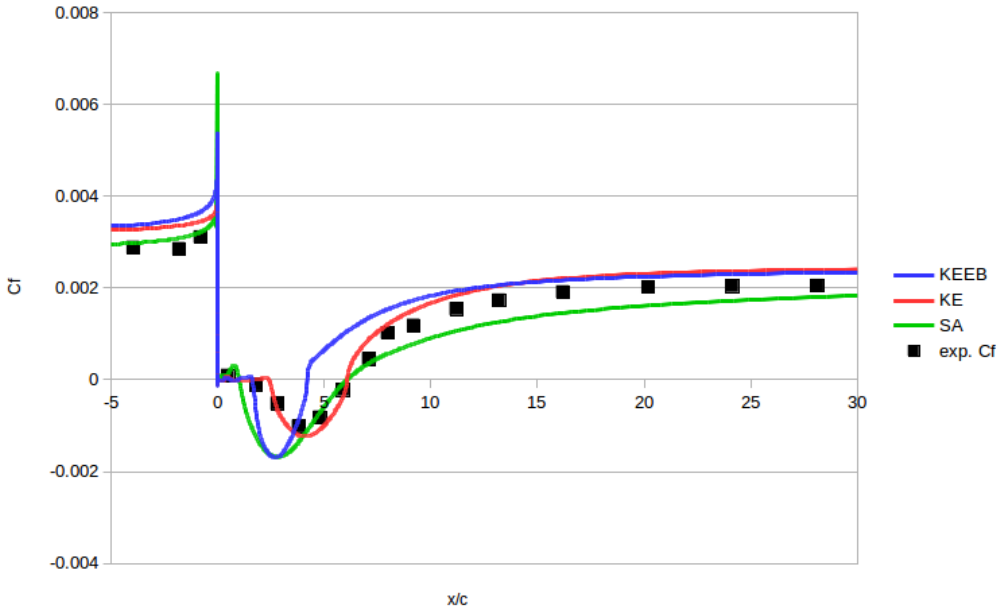

Figure 4. 24: Comparison of Skin-Friction distribution on the surface of the backward facing step.

Chapter 5: Development of a Transition Model

5.1 Introduction

The accurate prediction of transitional flow has remained a challenging problem in fluid dynamics for over a century. There has been lot of progress towards understanding of various mechanisms and fundamental concept behind transitional flows, nevertheless the accurate prediction of location and flow characteristics in transitional flow regime in complex 3D industrial applications such as flow over aircrafts, automobiles, wind turbines and in turbomachines, etc. remains a challenging area of research in fluid mechanics. In aerodynamics e.g., the location and process of the transitional flow over a wing have a significant impact on the lift characteristics of the wing and boundary layer separation. Therefore, accurate prediction of the transition flow is very important.

Currently for practical applications, the four-equation SST-Transition model developed by Menter et al. [18] is wieldy used by the industry. The three correlations used in this model are functions of the local transition onset momentum thickness Reynolds number. Recently, a three-equation model based on a transport equation for turbulence intermittency and the LCBT (local correlation-based transition-modelling) concept for triggering the transition onset was developed by Menter et al. [19]. In this paper, the local correlation-based transition-modelling is applied to the one-equation turbulence model based on k-ϵ closure [3]. The new transition model is first validated

by computing the ERCOFTAC benchmark transition flow fields over the T3 series of flat plates. The model is then tested on several other test cases namely the transitional flow past S809 airfoil, Aerospatiale-A airfoil and NLR-7301 two-element airfoil.

5.2 Derivation of Transition Model ($k\epsilon - \gamma$) based on One-Equation k-ϵ Closure

The one-equation $k-\epsilon$ model derived in chapter 4 is a one-equation eddy viscosity model derived from the two-equation $k-\epsilon$ closure. The one-equation $k-\epsilon$ model can predict the turbulent flows reasonably well but cannot model the laminar-turbulent transition process. Therefore, this model is modified to include the correlation-based intermittency equation γ based on the local correlation-based transition modelling concept. In one-equation $k-\epsilon$ model [3], the eddy viscosity is given by:

$$\widetilde{\nu_t} = C_\mu \frac{k^2}{\epsilon} \tag{5.1}$$

The transport equation for $\widetilde{\nu_t}$ which includes the intermittency equation γ in the production term can be written as:

$$\frac{D\widetilde{\nu_t}}{Dt} = c_1 D_1 E_\gamma \widetilde{\nu_t} S - c_2 E_{1e} + \frac{\partial}{\partial x_j}\left(\left(\nu + \frac{\widetilde{\nu_t}}{\sigma}\right)\frac{\partial}{\partial x_j}(\widetilde{\nu_t})\right) + P_{\widetilde{\nu_t}}^{lim} \tag{5.2}$$

$$\text{where} \quad \nu_t = D_2 \widetilde{\nu_t} \tag{5.3}$$

$$E_\gamma = min\left(C_\gamma \cdot \gamma, 1\right) \tag{5.4}$$

In Equation (5.2), an additional production term $P_{\widetilde{\nu_t}}^{lim}$ has been introduced to ensure

proper generation of $\widetilde{\nu_t}$ at transition points for arbitrarily low T_u levels. The expression for $P_{\widetilde{\nu_t}}^{lim}$ is given as:

$$P_{\widetilde{\nu_t}}^{lim} = 5W\, max(\gamma - 0.2, 0)\,(1.0 - \gamma)\, min\left(max\left(\frac{Re_v}{2420} - 1, 0\right), 3\right) ma\, x(3v - \widetilde{\nu_t}, 0) \quad (5.5)$$

The transport equation for the intermittency γ is formulated as:

$$\frac{\partial \rho\gamma}{\partial t} + \frac{\partial \rho u_j \gamma}{\partial x_j} = \frac{\partial}{\partial x_j}\left[\left(\mu + \frac{\mu_t}{\sigma_\gamma}\right)\frac{\partial \gamma}{\partial x_j}\right] + F_{length}\rho S\gamma(1-\gamma)F_{onset} - \rho c_{a2}\Omega\gamma F_{turb}(c_{e2}\gamma - 1) \quad (5.6)$$

In Equation (5.6), F_{onset} is used to trigger the intermittency production which is given by the following equations:

$$F_{onset1} = \frac{Re_v}{2.2Re_{\theta c}},\ F_{onset2} = min(F_{onset1},\ 2.0)\,, F_{onset3} = max\left(1 - \left(\frac{R_T}{6.0}\right)^3,\ 0\right) \quad (5.7)$$

$$F_{onset} = max(F_{onset2} - F_{onset3},\ 0) \quad (5.8)$$

$$F_{turb} = e^{-\left(\frac{R_T}{2}\right)^4},\ R_T = \frac{\nu_t}{v},\ Re_v = \frac{\rho d_w^2 S}{\mu} \quad (5.9)$$

The model constants are:

$$C_\gamma = 15.6,\ F_{length} = 150,\ c_{e2} = 50,\ c_{a2} = 0.06,\ \sigma_\gamma = 1.0 \quad (5.10)$$

The local turbulence intensity Tu_L is given by [19]:

$$Tu_L = min\left(100\,\frac{\sqrt{\frac{2\nu_t}{3}}}{\sqrt{\frac{S}{0.3}} * d_w},\ 100\right) \quad (5.11)$$

where d_w is the wall distance. In the original formulation of Tu_L obtained from Ref. [19], ν_t replaces turbulent kinetic energy k and ω and is replaced by ω ≈ S/0.3.

The formula for the pressure gradient parameter can be written as:

$$\lambda_{\theta L} = -7.57 \cdot 10^{-3} \frac{dV}{dy} \frac{d_w^2}{\nu} + 0.0128 \tag{5.12}$$

$Re_{\theta c}$ is given by [19]:

$$Re_{\theta c} = 100.0 + 1000.0 exp[-1.0 * Tu_L * F_{PG}] \tag{5.13}$$

F_{PG} is a correlation function of $\lambda_{\theta L}$:.

$$F_{PG} = \begin{cases} min\left(1 + C_{PG1}\lambda_{\theta L}, C_{PG1}^{lim}\right), \ \lambda_{\theta L} \geq 0 \\ min\left(1 + C_{PG2}\lambda_{\theta L} + C_{PG3} min[\lambda_{\theta L} + 0.0681, 0], C_{PG2}^{lim}\right), \ \lambda_{\theta L} < 0 \end{cases} \tag{5.14}$$

$$C_{PG1} = 14.68, C_{PG2} = -7.34, C_{PG3} = 0.0 \tag{5.15}$$

$$C_{PG1}^{lim} = 1.5, C_{PG2}^{lim} = 3.0 \tag{5.16}$$

In order to avoid negative value, F_{PG} is limited as:

$$F_{PG} = max(F_{PG}, 0) \tag{5.17}$$

The mean vorticity is given by:

$$W = \sqrt{2W_{ij}W_{ij}}, \qquad W_{ij} = \frac{1}{2}\left(\frac{\partial u_i}{\partial x_j} - \frac{\partial u_j}{\partial x_i}\right) \tag{5.18}$$

The coefficients used in one-equation eddy viscosity model in Equation (5.2) are as follows: $c_1 = 0.144$, $c_2 = 1.86$, $c_3 = 7$, $\sigma = 1$, $\kappa = 0.41$, $A^+ = 13$.

5.3 Validation Cases

This section shows the comparison of results computed by $k\epsilon$-γ transition model

(designated as KE-Transition model) and SST-Transition model. Several benchmark cases are computed to show the performance and accuracy of the new transition model. These cases include the ERCOFTAC T3 flat plate series, the S809 airfoil, the Aerospatiale-A airfoil, and the NLR-7301 two-element airfoil. All results are compared with experimental data for each case. The open-source computational fluid dynamics (CFD) code OpenFOAM is used to compute the flow fields.

5.3.1 Zero-Pressure Gradient Flat Plate Flow

Two zero pressure gradient flat plate cases (T3A, T3B) are computed, which have different free-stream velocities U_∞ and free-stream turbulence intensities Tu_∞ as given in Table 5.1. Figure 5.1 shows the mesh used in simulations for the two cases.

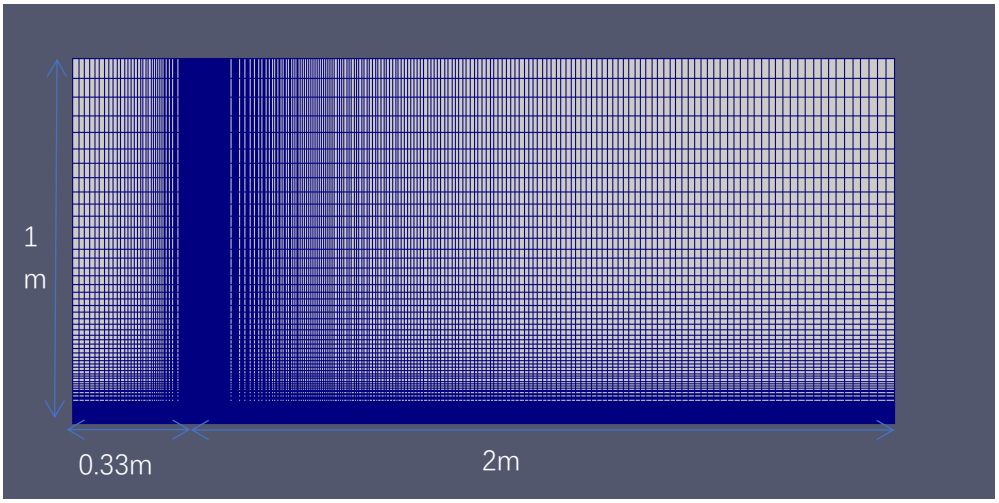

Figure 5. 1: Grid (221-191) in the computational domain for flow over flat plates

Table 5. 1: Inlet flow conditions for T3 series of flat plates

	U_∞ (m/s)	Tu_∞(%)	μ_T/μ	ρ (kg/m3)	μ (kg/m·s)
T3A	5.4	3.5	13.3	1.2	1.8e-5
T3B	9.4	6.5	100	1.2	1.8e-5

Figure 5.2 and Figure 5.3 show the computation results for wall skin-friction coefficient C_f vs. Reynolds number Re_x based on length in x direction and their comparison with experimental data [20]. Re_x is defined as:

$$Re_x = \frac{\rho_\infty U_\infty x}{\mu_\infty} \tag{5.19}$$

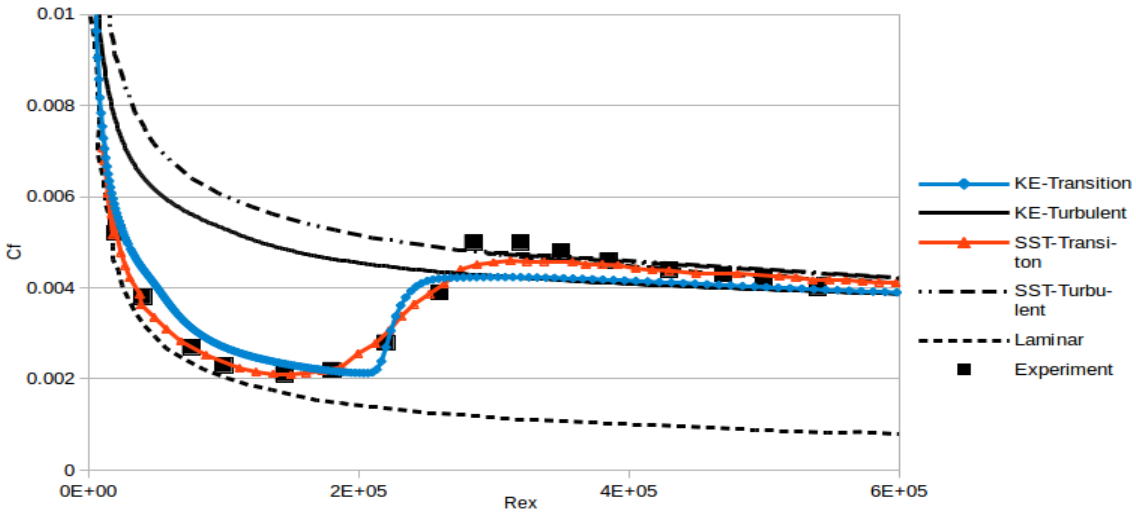

Figure 5. 2: Transitional flow past T3A flat plate

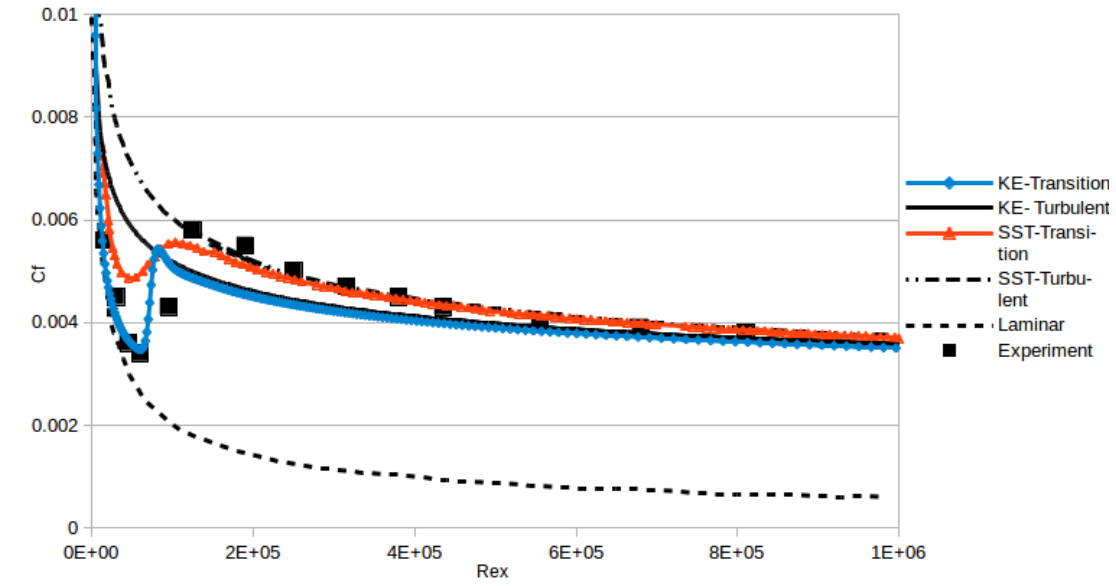

Figure 5. 3: Transitional flow past T3B flat plate

For T3A test case, Figure 5.2 shows that the SST-Transition model has better accuracy compared to the KE-Transition model. However, KE-Transition model performs better than the SST-Transition model in the transitional region of T3B test case. As these figures show that all transition models coincide with their original turbulence model in the fully turbulent flow region. It can be concluded that the difference between the KE-Transition model prediction and the experiment for the two test cases can be attributed to the behavior of the original turbulence model (one equation k-ϵ turbulence model).

5.3.2 Flow past S809 Airfoil

The S809 airfoil is an airfoil designed for wind energy applications at Mach 0.1[21]. The simulation was conducted at an angle of attack $\alpha = 10°$ at Reynolds number = 2×10^6. The free stream turbulence intensity is $Tu_\infty = 0.2\%$ and the viscosity ratio is $\frac{\nu_t}{\nu} = 10$.

Figure 5.4 shows the numerical results for the coefficient of pressure C_P on the S809 airfoil surface. The result computed by KE-Transition model is compared with the SST-Transition model and experimental data. It can be concluded that the result from KE-Transition model are in good agreement with the experimental data.

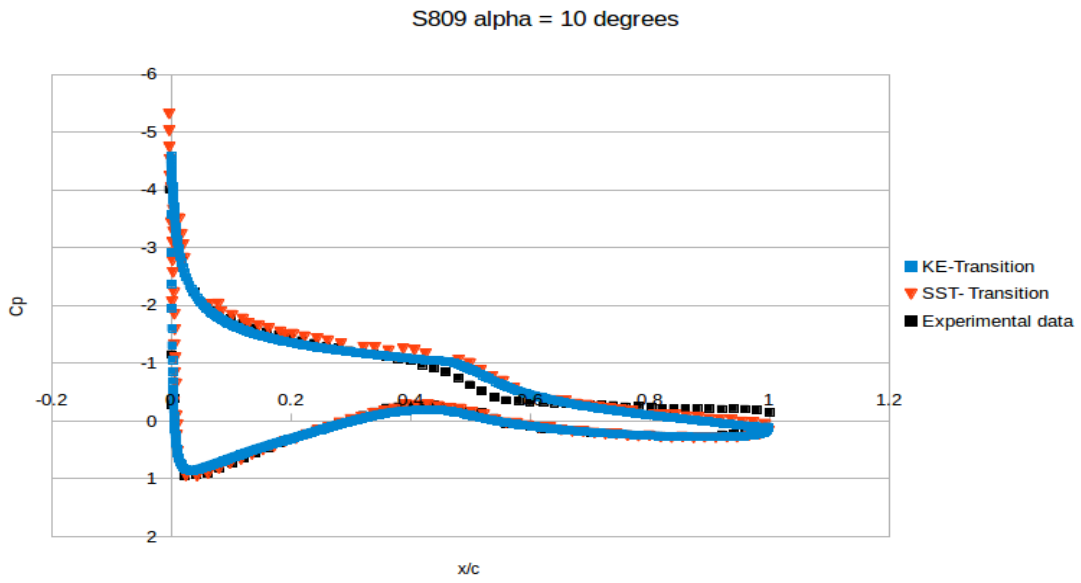

Figure 5. 4: Pressure coefficient on S809 airfoil at α = 10°.

5.3.3 Flow past Aerospatiale-A Airfoil

The Aerospatiale-A airfoil is a 0.6m chord airfoil designed for helicopter applications [22]. The simulation is performed at an angle of attack $\alpha = 13.1°$ and the Reynolds number is 2.07×10^6. In this case, the turbulence intensity is set at $Tu = 0.2\%$ with a viscosity ratio of $\frac{\nu_t}{\nu} = 10$ at the leading edge of the airfoil.

Figure 5.5 shows the numerical results computed by KE-Transition model for the coefficient of skin-friction C_f along the airfoil surface. The results are compared to the experimental data. Figure 5.5 shows that the KE-Transition model has reasonable agreement with the experimental data.

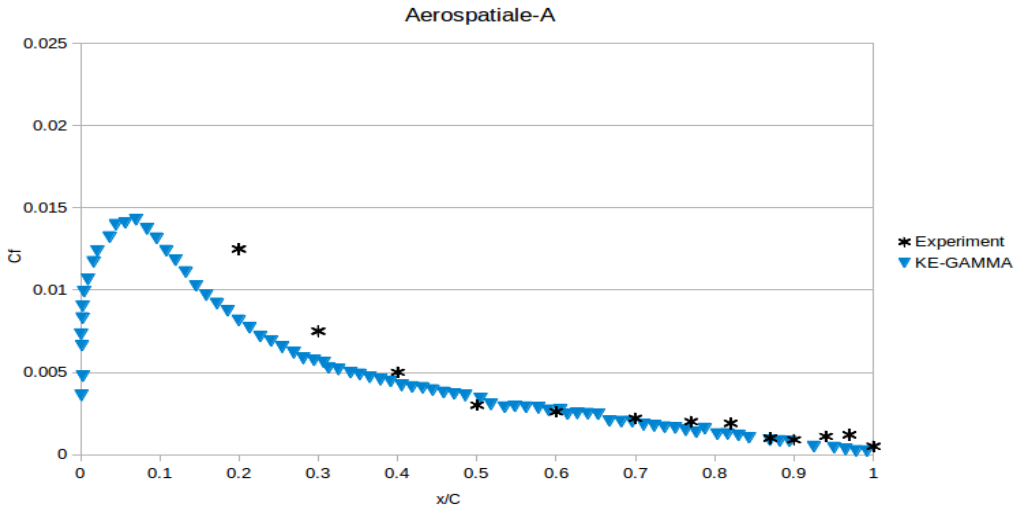

Figure 5. 5: Transitional flow past Aerospatiale-A airfoil at α = 13.1°.

5.3.4 Flow past NRL-7301 Two-Element Airfoil

This case is also commonly used for validation of transitional flow. The NLR-7301 two-element airfoil has a flap angle of 20° and the gap width between the flap and airfoil is 2.6% c (c is the chord of the main airfoil). The simulation is performed at α = 13.1° and the Reynolds number is 2.51 $x10^{6}$. In order to guarantee y+ is less than one, a very fine C mesh is applied near the airfoil surface.

Figure 5.6 shows the numerical results of pressure coefficients C_p computed by KE-Transition model compared to the experimental data [23]. Figure 5.7 shows the numerical results obtained from KE-Transition model for skin friction coefficients C_f on the airfoil and flap compared to the experimental data. As these figures show, the computational results computed by KE-Transition model are in good agreement with the experimental data

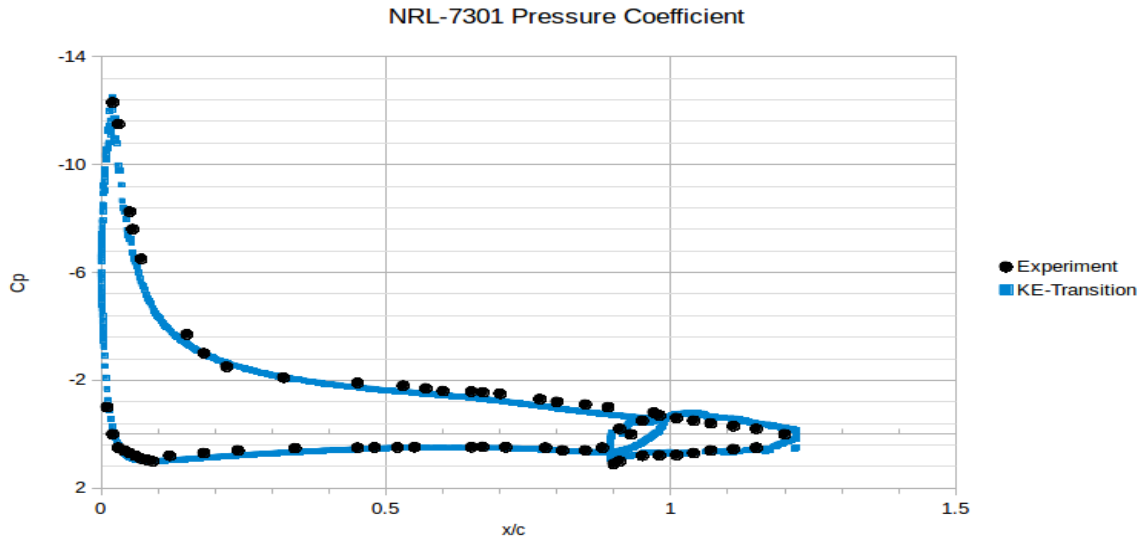

Figure 5. 6: Pressure coefficient on the surface of NLF-7301 airfoil and flap.

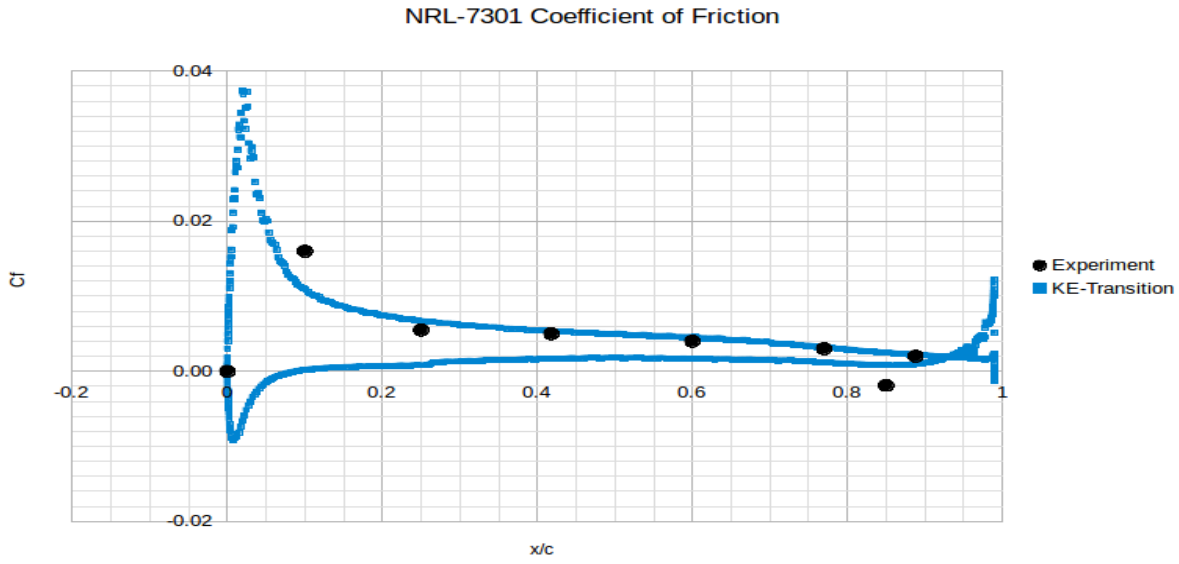

Figure 5. 7: Skin-friction coefficient on NLF-7301 airfoil.

Chapter 6: Summary and Future Work

6.1 Summary

It is shown that the proposed elliptic blending version of one-equation model based on $k-\epsilon$ closure (KEEB model) has better accuracy compared to the one-equation model based on $k-\epsilon$ closure (KE model). Both the models can predict the turbulent flow past a flat plate very well. However, for fully developed turbulent flow in a channel, KE model is not able to compute the buffer layer and log layer near the channel wall accurately. In contrast, the KEEB model shows significant improvement in calculation of the log layer for flow in the channel. Furthermore, KEEB model also shows slightly improved performance over KE model in calculating other benchmark test cases of flows with small regions of separation, namely the flow past NASA wall-mounted hump, flow over a backward facing step, flow in an asymmetric plane diffuser and flow over a periodic hill. Based on the results presented in this paper, it can be concluded that the KEEB model provides an improvement over the KE model by incorporation of elliptic blending in KE model for negligible additional computational cost.

A transition model is developed by integrating the one-equation turbulence model based on $k-\epsilon$ closure with the local correlation-based intermittency equation γ in OpenFOAM. The accuracy of the $k\epsilon$ - γ model (designated as KE-Transition model) was tested on several ERCOFTAC benchmark flat plate transition cases; the results showed that the two-equation KE-Transition model can predict the location and

process of laminar-turbulence transition flow quite well. The KE-Transition model can perform better than the SST-Transition model in the transition region for the T3B flat plate transition flow case. KE-Transition model was also used to compute the transition flow past S809 airfoil and Aerospatiale-A airfoil. It is shown that KE-Transition model can predict the experimental data very well. For the transition flow past the NRL-7301 two-element airfoil, the KE-Transition model also performed very well when compared to the experimental data. In general, the KE-Transition model was found to be accurate and efficient in predicting transitional flows past airfoils.

6.2 Future Work: Integration of an Algebraic Transition Model with One-Equation $k-\epsilon$ Turbulence Model (KE)

The KE-Transition model ($k\epsilon-\gamma$) contains the basic equation for $\widetilde{\nu_t}$ based on $k-\epsilon$ closure and contains one additional differential equation for intermittency γ. The model is quite good in accurately predicting the location of transition for different types of transitional flows. However, despite its accuracy, the model requires large amount of computational time to achieve a converged solution.

Algebraic transition models do not rely on differential equations for computing the intermittency characteristics but use algebraic relations which lead to less computational cost. This idea has been successfully implemented into two particular models, SA-BC [24] and $k-\omega$ KD [25]. Both models look promising based on the results presented in the corresponding papers. It is therefore worth applying this

approach to the one-equation $k-\epsilon$ turbulence model to create a new $k-\epsilon$ algebraic laminar-turbulent transition model.

The proposed equation for $\mathrm{k}-\epsilon$ algebraic laminar-turbulent transition model can be expressed as:

$$\frac{D\widetilde{\nu_t}}{Dt} = c_1 D_1 \widetilde{\nu_t} S\gamma - c_2 E_{1e} + \frac{\partial}{\partial x_j}\left(\left(\nu + \frac{\widetilde{\nu_t}}{\sigma}\right)\frac{\partial}{\partial x_j}(\widetilde{\nu_t})\right) \tag{6.1}$$

The equation for intermittency γ in Eq. (6.1) is given by:

$$\gamma = 1.0 - \exp\left(-\sqrt{Term_1} - \sqrt{Term_2}\right) \tag{6.2}$$

where

$$Term_1 = \frac{\max(Re_\theta - Re_{\theta c}, 0)}{\chi_1 Re_{\theta c}};\ Term_2 = \frac{\max(\nu_{BC} - \chi_2, 0)}{\chi_2} \tag{6.3}$$

are the trigging functions. $Term_1$ triggers onset of transition when $Re_\theta > Re_{\theta c}$ and the $Term_2$ function triggers the growth of intermittency inside the boundary layer. The auxiliary relations are:

$$Re_\theta = \frac{Re_\nu}{2.193};\ Re_\nu = \frac{\rho d_\omega^2}{\mu}\Omega;\ Re_{\theta c} = 803.73\,(\mathrm{Tu}_\infty + 0.6067)^{-1.027};\ \nu_{BC} = \frac{\nu_t}{U d_w} \tag{6.4}$$

The constants χ_1 and χ_2 need to be calibrated to ensure good agreement with the experimental data for all cases. Theoretically, this new model is more efficient for computation compared to the model described in chapter 5 in this thesis.

References

[1] Pope, S. B., "Turbulent flows." (2001): 2020. pp.3-5.

[2] Deardorff, James W., "A numerical study of three-dimensional turbulent channel flow at large Reynolds numbers". J. Fluid Mech., vol. 41, 1970, p.453-480.

[3] Menter, E. R., "Eddy Viscosity Transport Equations and their Relation to the $k-\epsilon$ Model," J. Fluids Eng, Vol. 119, No. 4, 1997, pp.876-884.

[4] Han, X., Wray, T. J., and Agarwal, R. K., "Application of a New DES Model Based on Wray-Agarwal Turbulence Model for Simulation of Wall-Bounded Flows with Separation," AIAA Paper 2017-3966, AIAA Aviation Forum, Denver, 5-9 June 2017.

[5] Rahman, M., Siikonen, T., and Agarwal, R. K., "Improved Low-Reynolds-Number One-Equation Turbulence Model," AIAA Journal, Vol. 49, 2011, pp.735-747.

[6] Shuai, S. and Agarwal, R. K., "A One-Equation Turbulence Model based on k-kL Closure," AIAA Paper 2019-1879, AIAA SciTech 2019 Conference, San Diego, CA, 7-11 January 2019.

[7] Spalart, P. R. and Allmaras, S. R, "A One Equation Turbulence Model for Aerodynamic Flows," AIAA Paper 1992-0439, 1992.

[8] Chien, K. Y., "Predictions of Channel and Boundary-Layer Flows with a Low-Reynolds-Number Turbulence Model," AIAA Journal, Vol. 20, No. 1, 1982, pp. 33-38.

[9] Wilcox, D. C., "Formulation of the k-ω Turbulence Model Revisited," AIAA Journal, Vol. 46, No. 11, 2008, pp. 2823-2838.

[10] Menter, F. R., "Two-Equation Eddy-Viscosity Turbulence Models for Engineering Applications," AIAA J., Vol. 32, No. 8, August 1994, pp. 1598-1605.

[11] NASA Langley Turbulence Modeling Resource website, http://turbmodels.larc.nasa.gov., (retrieved November 2017).

[12] Han, X., Rahman, M. M., and Agarwal, R. K., "Wall-Distance Free Wray-Agarwal Turbulence Model with Elliptic Blending," AIAA Paper 2018-4044, AIAA Aviation Forum, Atlanta, 25-29 June 2018.

[13] Lee, M., and Moser, R. D., "Direct Numerical Simulation of Turbulent Channel Flow Up to Re_tau = 5200,"J. Fluid Mech., Vol. 774, 2015, pp. 395-415.

[14] NPARC Alliance Verification and Validation Archive, https://www.grc.nasa.gov/WWW/wind/valid/whatsnew.html. (retrieved November 2017).

[15] European Research Community on Flow, Turbulence and Combustion (ERCOFTAC) Database, http://cfd.mace.manchester.ac.uk/ercoftac. (retrieved November 2017).

[16] Frohlich, J., Mellen, C. P., Rodi, W., Temmerman, L. and Leschziner, M. A., "Highly resolved large-eddy simulation of separated flow in a channel with streamwise periodic constrictions," J. Fluid Mech., Vol. 526, 2005, pp. 19-66.

[17] Bruice, C. and Eaton, J. K., "Experimental Investigation of Flow through an Asymmetric Plane Diffuser," Stanford Univ. Dept. of Mechanical Engineering, Thermoscience Division Rept. TSD-107, Stanford, CA, 1997.

[18] Menter, F. R., Langtry, R. B., Likki, S. R., Suzen, Y. B., Huang, P. G., and Völker, S., "A Correlation-Based Transition Model Using Local Variables — Part I: Model Formulation," ASME Journal of Turbomachinery, Vol. 128, July 2006, pp. 413-422.

[19] Menter, F. R., Langtry, R.B., Smirnov, P. E. and Liu, T., "A One-Equation Local Correlation-Based Transition Model," Flow, Turbulence and Combustion, Vol. 5, No. 4, 2015, pp. 583-619.

[20] ERCOFTAC (European Research Community on Flow, Turbulence and Combustion) [online database], URL: http://ercoftac.mech.surrey.ac.uk/(retrieved 15 Feb 2008).

[21] Somers, D. M., "Design and Experimental Results for the S809 Airfoil," Airfoils Inc., State College, PA, Jan 1997.

[22] Chaput, E., “Chapter III: Application-Oriented Synthesis of Work Presented in Chapter II.” Notes on Numerical Fluid Mechanics, Vol. 58, 1997, pp. 327-346.

[23] Van den Berg, B., “Boundary Layer Measurements on a Two-Dimensional Wing with Flap,” Report No: NLR TW 79009U, National Aerospace Laboratory, Netherlands, 1979.

[24] Cakmakcioglu, Samet Caka, Onur Bas, and Unver Kaynak., "A Correlation-Based Algebraic Transition Model," Proceedings of the Institution of Mechanical Engineers, Part C: J. of Mech. Engineering Science 232, no. 21 (2018): 3915-3929.

[25] Kubacki, Slawomir, and Erik Dick., "An Algebraic Model for Prediction of Bypass and Separation-induced Transition in Turbomachinery Boundary Layers." In 11th International ERCOFTAC Symposium on Engineering Turbulence Modelling and Measurements, pp. 1-6. University of Palermo, 2016.

Vita

Cheng Peng

EDUCATION

M.S. in Mechanical Engineering, Department of Mechanical Engineering and Materials Science, Washington University in St. Louis, Saint Louis, MO.
2017-2019

B.S. in Energy and Power Engineering, Department of Energy Power and Mechanical Engineering, North China Electric Power University, Beijing. 2013-2017

PUBLICATIONS

Cheng Peng, Xu Han and Ramesh Agarwal. "A New One Equation Turbulence Model Based on $\boldsymbol{k} - \boldsymbol{\varepsilon}$ Closure with Elliptic Blending," AIAA 2019-1880, AIAA Scitech 2019 Forum, San Diego, CA, 7-11, January 2019.

Cheng Peng and Ramesh Agarwal. "Development of a Transition Model Based on One-Equation k-epsilon Closure," 2019 AIAA Aviation and Aeronautics Forum and Exposition, Dallas, TX, 17-21 June 2019.

PROFESSIONAL MEMBERSHIP

American Institute of Aeronautics and Astronautics (AIAA)